

# Contrail Cirrus Climate Impact: From Radiative Forcing to Surface Temperature Change

MARIUS BICKEL<sup>1</sup>,<sup>a</sup> MICHAEL PONATER,<sup>a</sup> ULRIKE BURKHARDT,<sup>a</sup> MATTIA RIGHI,<sup>a</sup> JOHANNES HENDRICKS,<sup>a</sup> AND PATRICK JÖCKEL<sup>a</sup>

<sup>a</sup> *Deutsches Zentrum für Luft- und Raumfahrt, Institut für Physik der Atmosphäre, Oberpfaffenhofen, Germany*

(Manuscript received 13 May 2024, in final form 26 December 2024, accepted 14 January 2025)

**ABSTRACT:** Contrail cirrus has been regarded as the most important individual component of aviation-induced global climate impact, a conclusion prompted by radiative forcing estimates from a variety of models. However, there have been indications of a reduced effective radiative forcing of contrail cirrus with respect to its instantaneous radiative impact, as well as indications of a reduced contrail efficacy to force surface temperature changes. Here, we present a set of global climate model simulations driven by either upscaled contrail cirrus or a CO<sub>2</sub> increase, first with prescribed and then with interactive sea surface temperature, yielding self-consistent results for forcings, feedbacks, and climate sensitivity. If contrail cirrus and CO<sub>2</sub> induce the same classical (stratosphere adjusted) radiative forcing, we find the contrail cirrus effective radiative forcing reduced to about 55% compared to that from CO<sub>2</sub>, qualitatively confirming previous results. The surface temperature response per unit effective radiative forcing (the climate sensitivity parameter) is also smaller (reduced to about 40%) for contrail cirrus. In total, the simulations indicate an efficacy value as low as 0.21 for contrail cirrus, with an estimated statistical uncertainty between 0.10 and 0.32, while consolidated knowledge to quantify the respective systematic uncertainty is currently lacking. Our results indicate a much smaller relative contrail cirrus impact on global warming than classical or even effective radiative forcing estimates suggest. The analysis of radiative adjustments and feedbacks reveals a major role of natural clouds in driving the differences in the response behavior. We discuss consequences of the results for aviation climate impact assessments and promising further research directions.

**SIGNIFICANCE STATEMENT:** To date, the impact of contrail cirrus on global surface temperature change is largely unknown. Based on a set of climate model simulations, this study provides a first determination of respective key parameters explaining global surface warming (climate sensitivity and efficacy). The obtained climate sensitivity is lower for contrail cirrus than for CO<sub>2</sub>. The simulations were further examined by feedback analysis to identify the radiative processes which are most relevant for the exceptionally low efficacy of contrail cirrus radiative forcing to induce surface temperature changes.

**KEYWORDS:** Contrails; Climate sensitivity; Feedback; Radiative forcing; Surface temperature; Climate models

## 1. Introduction

In the context of anthropogenic climate change, the contribution from aircraft emissions has always attracted special attention (e.g., Penner et al. 1999). This is mainly motivated by large economic aviation growth rates in the past, which are expected to continue in the future despite pausing socioeconomic developments like the recent COVID-19 crisis (e.g., Grewe et al. 2021). Consequently, the global aviation climate effect has been regularly reviewed over the decades (Penner et al. 1999; Sausen et al. 2005; Lee et al. 2009; Brasseur et al. 2016; Kärcher 2018; Lee et al. 2021), and the respective

contributions from individual impact components have been assessed. The relevant contributions originate from CO<sub>2</sub>, nitric oxide, aerosol, and water vapor emissions and from contrail cirrus (Lee et al. 2010). Since Burkhardt and Kärcher (2011) provided the first simulation of contrail cirrus and its radiative forcing (RF), it has frequently been rated as the most important aviation climate impact component. Contrail cirrus develops from aircraft-emitted water vapor and aerosols. It may spread and prevail in the upper atmosphere for many hours under favorable atmospheric conditions, as known from both observations and numerical modeling (e.g., Minnis et al. 1998; Kästner et al. 1999; Boucher 2011; Schumann 2012; Bock and Burkhardt 2016a; Kärcher 2018). The relative climatic importance of the various aviation impact components has usually been quantified and ranked in terms of RF as a metric, following a long-standing common practice in climate research (e.g., Ramaswamy et al. 2018). Yet, in order to optimally fulfill its purpose as a global climate impact metric (Fuglestedt et al. 2010), RF has to be a good linear proxy for the expected global mean surface temperature change ( $\Delta T_{\text{surface}}$ ), at least for small perturbations of the climate system:

$$\Delta T_{\text{surface}}^i = \lambda_{\text{RF}}^i \times \text{RF}^i. \quad (1)$$

<sup>1</sup> Denotes content that is immediately available upon publication as open access.

Supplemental information related to this paper is available at the Journals Online website: <https://doi.org/10.1175/JCLI-D-24-0245.s1>.

Corresponding author: Marius Bickel, marius.bickel@dlr.de

DOI: 10.1175/JCLI-D-24-0245.1

© 2025 American Meteorological Society. This published article is licensed under the terms of the default AMS reuse license. For information regarding reuse of this content and general copyright information, consult the AMS Copyright Policy ([www.ametsoc.org/PUBSReuseLicenses](http://www.ametsoc.org/PUBSReuseLicenses)).

Experience has shown that this is not always the case. For many nonhomogeneously distributed climate forcings, the induced global mean surface temperature response per unit radiative forcing [the climate sensitivity parameter  $\lambda$  in Eq. (1)] deviates from that of  $\text{CO}_2$  (e.g., Hansen et al. 2005; Stuber et al. 2005; Shindell 2014). In particular, this has been found true for line-shaped contrails (Ponater et al. 2005; Rap et al. 2010).

Hansen et al. (2005) have coined the term “efficacy” [ $f^i$  in Eq. (2)] for assessing the surface temperature change due to perturbations of different forcings  $i$  that are associated with a climate sensitivity parameter different from that of  $\text{CO}_2$ :

$$\Delta T_{\text{surface}}^i = f_{\text{RF}}^i \times \lambda_{\text{RF}}^{\text{CO}_2} \times \text{RF}^i. \quad (2)$$

As a possibility to deal with the conceptual problem of varying efficacies, a new RF definition has been developed over the years, as explained by, e.g., Myhre et al. (2013) and Ramaswamy et al. (2018). From extensive experience with climate model simulations, the so-called effective RF (ERF) has been suggested as a better proxy for global mean surface temperature change, bringing forcing efficacies closer to unity. In this framework, the RF according to the original definition is replaced by ERF in Eq. (2):

$$\Delta T_{\text{surface}}^i = f_{\text{ERF}}^i \times \lambda_{\text{ERF}}^{\text{CO}_2} \times \text{ERF}^i. \quad (3)$$

Accordingly, Eq. (1) can be rewritten within the ERF framework as

$$\Delta T_{\text{surface}}^i = \lambda_{\text{ERF}}^i \times \text{ERF}^i. \quad (4)$$

As a consequence, in the more recent IPCC reports a switch to ERF as the preferred metric was made (Forster et al. 2021) for an improved quantitative comparison between individual climate forcings with respect to their impact on surface temperature. This switch was also adopted in the most recent aviation impact study by Lee et al. (2021) who compiled relevant research work on contrail cirrus radiative forcing (Burkhardt and Kärcher 2011; Bock and Burkhardt 2016b; Chen and Gettelman 2013; Schumann et al. 2015; Bickel et al. 2020), providing a best estimate for contrail cirrus ERF of  $57 \text{ mW m}^{-2}$  for the year 2018, and proposing an ERF/RF ratio of 0.42. The ERF/RF value of Lee et al. (2021) was identified with the contrail cirrus efficacy in the RF framework [Eq. (2)], but such identity is strictly valid under certain assumptions only (Ponater et al. 2021; Lee et al. 2021, their appendix C), which need to be verified in coupled atmosphere–ocean simulations. Such a direct simulation of contrail cirrus–induced surface temperature change, and thus, a targeted calculation of contrail cirrus efficacy is not yet available. The present paper aims to close this gap in aviation climate impact research. The path toward this objective is illustrated in Fig. 1.

Determining the efficacy for contrail cirrus (or any other non- $\text{CO}_2$  forcing) is a three-step effort starting from the instantaneous radiative effect (mostly including the adaption of the stratosphere, the so-called stratospheric temperature adjustment; see Ramaswamy et al. 2018). This so-called stratosphere adjusted RF ( $\text{RF}_{\text{adj}}$ ) will be called the “classical RF”

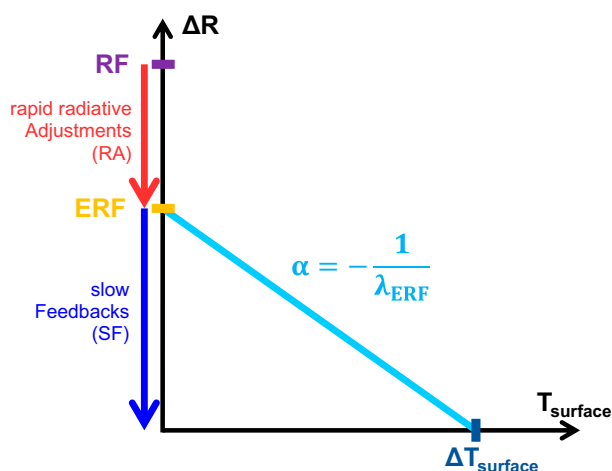


FIG. 1. Illustration of the link between surface temperature change ( $\Delta T_{\text{surface}}$ ) and RFs. The difference between the classical RF and ERF can be explained by rapid radiative adjustments (RAs) (red arrow, negative in this example). SFs (dark blue arrow) develop as a reaction to the surface temperature change. The feedback parameter  $\alpha$  is described by the slope of the light blue line.

within the framework of this paper. We note that the contrail RF has often been quantified by using the alternative definition of instantaneous RF ( $\text{RF}_{\text{inst}}$ ) in earlier papers (e.g., Minnis et al. 1999; Rädcl and Shine 2008; Schumann et al. 2012; Chen and Gettelman 2013), yet  $\text{RF}_{\text{inst}}$  and  $\text{RF}_{\text{adj}}$  (though considerably different in the  $\text{CO}_2$  case) exhibit nearly identical values in the contrail case (Dietmüller et al. 2016; Bickel 2023). The second step is to calculate the ERF, which in contrast to the classical RF includes the radiative effect of all rapid adjustments in the atmosphere that develop on a short time scale, before the slowly reacting ocean temperature starts to change (see also Hansen et al. 2005, their Fig. 2d). These first two steps, for which simulations with fixed sea surface temperature (FSST) are sufficient, have been described in Bickel et al. (2020). To achieve our main objective, we follow their path by complementing FSST simulations with corresponding simulations using an interactive mixed layer ocean (MLO). In this third step, the equilibrium surface temperature response, forced by the ERF and modulated by slow atmospheric feedbacks (see also Hansen et al. 2005, their Fig. 2e), is determined and the resulting climate sensitivity parameter for contrail cirrus [Eq. (4)] can be derived. An equivalent set of simulations with a  $\text{CO}_2$  forcing of similar magnitude then allows to calculate the contrail cirrus efficacy.

Taking care for the statistical significance (and, thus, the interpretability) of the simulated key parameters is a matter of specific relevance in the contrail cirrus case. Classical RF can be calculated with high statistical accuracy by applying the double radiation calling technique within one model simulation (Stuber et al. 2001; Chung and Soden 2015a; Dietmüller et al. 2016). In this context, it should be noted that the large uncertainty bar attributed by Lee et al. (2021, their Fig. 3) to the classical RF of contrail cirrus is based on systematic uncertainties, estimated from intermodel differences and partly

derived by expert judgment (for further details see [Lee et al. 2021](#), their appendix E). In contrast to the classical RF, both the ERF and global mean temperature change (as well as the underlying radiative adjustments and feedbacks) are additionally associated with a substantial level of statistical uncertainty (e.g., [Forster et al. 2016](#); [Smith et al. 2018](#)) because they have to be calculated as the difference between two independent free-running climate model simulations with considerable internal variability (noise). To ensure a sufficient signal-to-noise ratio, we will apply the method of scaling the air traffic volume and, thus, the contrail cirrus forcing to the required magnitude, i.e., we adopt the approach successfully tested by [Bickel et al. \(2020\)](#). More details of the methodology are described in [section 2](#).

In this paper, the intention is not to establish new estimates of the classical RF for contrail cirrus; those were presented and discussed by [Bock and Burkhardt \(2016b, 2019\)](#) for 2006 and 2050 aviation conditions, respectively, from a series of self-consistent simulations using the ECHAM5 model. Rather, we use the classical RF from the scaled simulations as the starting point to derive the parameters relevant for global mean surface temperature response, i.e., the ERF/RF factor, climate sensitivity parameter, and efficacy ([sections 3 and 4](#)). These will be addressed in relation to the rapid and slow feedbacks that may explain the origin of a different response behavior in contrail cirrus and CO<sub>2</sub>-driven climate change simulations. A discussion of consequences that these results may have for the assessment of aviation climate impact and contrail mitigation studies concludes the present study.

## 2. Model, simulations, and feedback analysis

### a. Climate model EMAC

In contrast to previous work on the contrail cirrus ERF, performed with the ECHAM5 global climate model ([Bickel et al. 2020](#); [Ponater et al. 2021](#)), the simulations for the present study were all conducted with the ECHAM/Modular Earth Submodel System (MESSy) Atmospheric Chemistry (EMAC) model ([Jöckel et al. 2010](#)). The MESSy infrastructure (version used here: 2.54) features a modular structure with a wide range of parameterizations and submodels (e.g., multiple cloud modules) that facilitate flexible creation of consistent, target-oriented, model setups. A ready to use and extensively tested MLO that is required for the surface temperature change simulations was the main motivation to switch to the EMAC model environment ([Kunze et al. 2014](#)). In addition, EMAC is far more flexible in terms of setup modifications and handling additional diagnostic features, and it will, e.g., provide an ideal basis for later nudged simulations (e.g., [Jöckel et al. 2006](#); [Lelieveld et al. 2007](#); [Jöckel et al. 2016](#)). This technique could potentially improve the signal-to-noise ratio for calculating the contrail cirrus ERF and climate response, as demonstrated by [Chen and Gettelman \(2013\)](#) and [Gettelman et al. \(2021\)](#). However, as explained in the introduction, we decided to use the alternative method of scaling the air traffic volume for our simulations, because it has not yet been clarified how (or to which extent) the nudging method affects rapid adjustments and cloud sensitivities (e.g., [Forster et al.](#)

[2016](#); [Lin et al. 2016](#); [Sun et al. 2019](#)). More important, it is largely unknown whether nudging may modify the climate sensitivity of an interactive atmosphere–ocean model as used for the present paper.

For the objectives pursued here, the contrail cirrus module (CCMod) parameterization ([Bock 2014](#); [Bock and Burkhardt 2016a,b](#)) was implemented into the cloud module developed by [Kuebbeler et al. \(2014\)](#), hereafter **K14**. **K14** represents an evolution of the [Lohmann and Ferrachat \(2010\)](#), hereafter **LF10** cloud module which was used in the ECHAM5 simulations of [Bickel et al. \(2020\)](#). The **K14** scheme was implemented in EMAC by [Righi et al. \(2020\)](#) and coupled by [Kaiser et al. \(2019\)](#) to the Modal Aerosol Dynamics Model for Europe, adapted for global applications, 3rd generation (MADE3) aerosol submodel. The main features of **K14** are a revised ice microphysical scheme for cirrus clouds, which is based on nine different aerosol modes from MADE3. Note that the ECHAM5–Hamburg Aerosol Model (HAM) aerosol module ([Stier et al. 2005](#)) had been used in the ECHAM5–CCMod model ([Bock and Burkhardt 2016a](#); [Bickel et al. 2020](#)) instead. In EMAC–CCMod, nucleation of ice crystals in natural cirrus clouds is represented by a parameterization for homogeneous and heterogeneous freezing, which may also compete with each other ([Kärcher et al. 2006](#)). The extensions of [Bier and Burkhardt \(2019\)](#) for CCMod were deliberately omitted in order to remain consistent with our previous simulations performed with the ECHAM5 model (see [Bickel et al. 2020](#)).

To implement CCMod in EMAC, the **K14** cloud scheme had to be adapted in the same way as the **LF10** scheme was adapted by [Bock and Burkhardt \(2016a\)](#). The [Sundqvist \(1978\)](#) fractional cloud cover and the associated saturation adjustment were reintroduced (for a more detailed description, see [Bickel 2023](#), sections 3.1.2 and 3.1.3). As a consequence of these changes, the model needed to be retuned in order to keep the radiative imbalance sufficiently small (within  $\pm 0.5 \text{ W m}^{-2}$ ), which is mandatory for coupling the MLO. The tuning process followed common techniques ([Mauritsen et al. 2012](#); [LF10](#); [Righi et al. 2020](#)). However, some of the parameters usually tuned to yield a radiation balance closure are prone to affect the contrail cirrus itself, which had to be avoided. The choice of tuning parameters and an evaluating comparison of global mean key parameters with observations, with a focus on natural cloud and contrail cirrus properties (e.g., liquid and ice water content), can be found in [Bickel \(2023\)](#), appendix A, Tables A1 and A2). The ice supersaturation frequency derived with EMAC, which specifies the maximum possible extent of persistent contrail cirrus cover, was analyzed in detail and agrees closely with ECHAM5–CCMod (see [Bickel 2023](#), appendix A, Fig. A1). The successful tuning was confirmed by two test simulations for 2006 air traffic, yielding almost identical classical RFs of  $60.0 \text{ mW m}^{-2}$  for ECHAM–CCMod and  $60.7 \text{ mW m}^{-2}$  for EMAC–CCMod.

Note that, identical to the previously performed simulations with ECHAM5 ([Bickel et al. 2020](#); [Ponater et al. 2021](#)), a resolution of T42L41 (corresponding to a horizontal resolution of  $2.8^\circ$ ) was chosen, and (except for **K14** replacing **LF10** and MADE3 replacing HAM) the same set of physical parameterizations was used. The chemical scheme already

tested in connection with the use of MADE3 was adopted from Righi et al. (2020).

Key features in the CCMod parameterization set are use of the two-moment cloud scheme (with ice water content and ice crystal number concentration as prognostic variables), which allows to describe size-dependent microphysical processes and to derive cirrus optical properties like optical depth and ice crystal size from the simulated variables (Bock and Burkhardt 2016a,b). Contrail formation and contrail cirrus development are embedded in the hydrological cycle and compete for available ambient water against natural cirrus (Burkhardt and Kärcher 2009). Further parameterized processes in CCMod are volume growth due to turbulent diffusion and sedimentation, spreading from wind shear, deposition, and loss of ice crystals from sublimation, sedimentation, and precipitation (for more details see Bock and Burkhardt 2016a,b).

### b. Feedback analysis

To get a deeper understanding of the processes controlling the radiative impact and climate response of contrail cirrus and CO<sub>2</sub> on Earth's atmosphere and surface, all our simulations were further examined by feedback analysis. As in our previous work (Bickel et al. 2020; Ponater et al. 2021), we use the partial radiative perturbation (PRP) framework (e.g., Colman and McAvaney 1997; Klocke et al. 2013). In contrast to the more common radiative kernel method (e.g., Soden et al. 2008), the PRP method directly calculates the cloud radiative feedbacks in full consistency with the climate model simulations (Zelinka et al. 2012). This is the optimal approach for our study, as cloud feedbacks are of high relevance with respect to contrail cirrus (Burkhardt and Kärcher 2011; Bickel et al. 2020). For this purpose, the previously applied feedback tool for ECHAM5 (Klocke et al. 2013; Rieger et al. 2017; Bickel et al. 2020) was recoded, extended (e.g., by an aerosol feedback contribution), and adapted to the EMAC model environment for this study.

The same technical PRP analysis tool was used to determine, first, RAs from FSST simulations and, second, slow feedbacks (SFs) from the interactive ocean simulations. While RAs explain the difference between the classical and effective RFs, the SFs restore the radiative equilibrium at the top of the atmosphere (TOA) as a reaction to surface temperature change and associated adaptations (Fig. 1):

$$\text{ERF} = \text{RF} + \sum_n \text{RA}_n, \quad (5)$$

$$\text{ERF} + \sum_n \text{SF}_n \approx 0. \quad (6)$$

Individual RA and SF components (labeled by index  $n$ ) were determined for feedback processes attributable to changes in mean surface and tropospheric temperatures (Planck feedback), tropospheric vertical temperature gradient (lapse rate feedback), water vapor mixing ratio (water vapor feedback), cloud microphysical and macrophysical properties (cloud feedback), and surface albedo (albedo feedback). To keep the residuum within the forcing–feedback balance as small as possible, we also added specific terms covering changes in the stratospheric temperature

(stratospheric temperature feedback) and aerosol properties (aerosol feedback). A direct quantitative comparison of corresponding RAs between contrail cirrus and CO<sub>2</sub> is enabled in our setup by using similarly sized classical radiative forcings. Comparison is not so straightforward for the SFs, if the effective radiative forcings of both forcing agents differ. However, this problem is eliminated by normalizing the SFs with the surface temperature change to yield the so-called feedback parameters (FPs):

$$\text{FP}_n = \frac{\text{SF}_n}{\Delta T_{\text{surface}}}. \quad (7)$$

Note that the sum of all individual FPs yields the total feedback parameter  $\alpha$ , which is the negative inverse of the climate sensitivity parameter in the ERF framework ( $\lambda_{\text{ERF}}$ ) known from Fig. 1 and Eq. (4):

$$\alpha = \sum_n \text{FP}_n = -\frac{1}{\lambda_{\text{ERF}}}. \quad (8)$$

Comparing the differences of these key parameters between the two forcing mechanisms allows to reveal specific physical processes controlling their forcing, feedback, and response relationship.

### c. Simulations concept

As stated above, all simulations for the present study were performed with the EMAC model, in which the CCMod parameterization has been implemented (referred to as EMAC–CCMod in the present paper). Still some boundary conditions and guiding ideas were adopted from our previously conducted simulations with the ECHAM5–CCMod model by Bickel et al. (2020). The reference simulations represent a state with the near present-day sea surface temperature, a CO<sub>2</sub>-mixing ratio of 348 ppmv, and no contrails. Prescribed sea surface temperatures were taken from observations for year 2003, as provided by Rayner et al. (2003). The basis of contrail initialization is an air traffic inventory provided by Wilkerson et al. (2010). This dataset has been created, among other inventories, for a future scenario of the year 2050 and contains air traffic density (flown distances) and corresponding water emissions. In the year 2050, air traffic is expected to be quadrupled relative to the year 2006 (Bock and Burkhardt 2019). In addition to using this inventory, the performed simulations were further scaled, which means that the air traffic density as well as water vapor emissions were increased by the same factor.

Compared to CO<sub>2</sub> emissions, which become relatively well mixed throughout the whole atmosphere, air traffic is characterized by its inhomogeneous distribution (cf. to Bickel et al. 2020, their Fig. 5a). About 92% of the flights take place over the Northern Hemisphere with hotspots over Europe, the United States, and China. This is reflected in the classical RF geographical distribution (Bock and Burkhardt 2019, their Fig. 2), which shows a corresponding and statistically robust spatial structure. However, as has been pointed out by Bickel et al. (2020, see their Fig. 1), the statistical uncertainties (resulting from the internal model variability) increase drastically

TABLE 1. Summary of simulations performed for the present study and the respective simulation lengths. Note that only the number of evaluated years is shown (spinup phases excluded). Contrail cirrus simulations are labeled as ATR-12, indicating the underlying 12-fold scaling of the year 2050 air traffic inventory. ATR-12 was complemented by CO<sub>2</sub> increase simulations with a classical RF of similar magnitude (CO2-12). In addition, CO<sub>2</sub>-doubling simulations were performed (CO2-2×). Simulations with FSST are used to determine both the classical RF and the ERF. Simulations with coupled MLO are used to assess the corresponding surface temperature changes.

	Reference (years)	ATR-12 (years)	CO2-12 (years)	CO2-2× (years)
FSST simulations (objective: RF and ERF)	30	30	30	30
MLO simulations (objective: $\Delta T_{\text{surface}}$ )	40	40	40	25

when the ERF is to be determined. For this reason, we have retained the 12 times scaling of the air traffic dataset, as established by Bickel et al. (2020), for the simulations presented here. In addition to increasing the signal-to-noise ratio, this enables a direct comparison between the results of this paper with those of Bickel et al. (2020). We note that, if RF is in the range of about 50 mW m<sup>-2</sup> or below, attempts to use global climate models for simulating a statistically significant surface temperature response have turned out to be unsuccessful (e.g., Huszar et al. 2013).

One main objective of the present study is to run a consistent pair of radiative forcing (classical RF as well as ERF) and surface temperature change simulations, induced by contrail cirrus, in order to determine the climate sensitivity parameter [cf. to Eqs. (1) and (4)]. For this purpose, two different types of simulation setups were utilized:

- 1) simulations with prescribed sea surface temperatures to derive the radiative forcings and
- 2) simulations with interactive ocean to determine the surface temperature change.

As climate sensitivity peculiarities of individual forcings are usually assessed with respect to a reference CO<sub>2</sub> perturbation [see Eq. (2)], our investigations are complemented by corresponding CO<sub>2</sub> increase simulations.

#### 1) RADIATIVE FORCING SIMULATIONS

As motivated by Bickel et al. (2020), the ERFs were determined using the FSST approach (Shine et al. 2003; Hansen et al. 2005). The FSST method ensures the full development of all rapid radiative adjustments (e.g., compared to the nudging approach, see Forster et al. 2016), while keeping the statistical uncertainties within reasonable limits [e.g., relative to regression based methods, compare to Gregory et al. (2004)]. Technically, the ERF based on the FSST method is calculated from two independent simulations, one without perturbation (reference) and one with perturbation (experiment). In contrast, the classical RF can be derived within one simulation, using the radiative double calling technique as described by Stuber et al. (2001). As one consequence of the flexible setup of the MESSy radiation (RAD) submodel (Dietmüller et al. 2016), the classical radiative forcing can be calculated as an integral part of the ERF experiment (see Bickel 2023, for technical details).

The contrail cirrus experiment with the underlying 12 times scaled 2050 air traffic inventory (in the following referred to as ATR-12) was supplemented by two CO<sub>2</sub> increase scenarios.

The first one uses similarly sized classical radiative forcing as in ATR-12 (in the following referred to as CO2-12) to enable a most meaningful comparison of climate sensitivity parameters (Hansen et al. 2005; Stuber et al. 2005). The second one is a common CO<sub>2</sub>-doubling simulation (in the following referred to as CO2-2×), mainly as a backup to ensure the significance of feedback and response results with a low signal-to-noise ratio in CO2-12 (see Bickel et al. 2020). The CO<sub>2</sub> increase to imitate the classical RF of the contrail cirrus experiment turned out to be +56 ppmv, while the CO<sub>2</sub>-doubling simulation was based on a CO<sub>2</sub> mixing ratio of 696 ppmv (2 × 348 ppmv reference value). To derive the rapid radiative adjustments, all three experiments were analyzed by the PRP feedback analysis (see section 2). In total, 120 years (4 × 30 years) of RF-targeted simulations were performed (see Table 1).

#### 2) SURFACE TEMPERATURE CHANGE SIMULATIONS

To determine the surface temperature change induced by contrail cirrus and by the two CO<sub>2</sub> perturbations mentioned above, the prescribed sea surface temperature climatology was replaced by an interactive MLO, following the common technical procedure using a surface flux correction method that keeps the simulated sea surface and sea ice distribution in the reference run close to the respective conditions in the FSST case (e.g., Kunze et al. 2014; Stecher et al. 2021).

In total, four surface temperature change simulations were performed: reference (no perturbation), ATR-12 (experiment with 12 times scaled air traffic), CO2-12 (experiment with +56 ppmv CO<sub>2</sub>, to be compared to ATR-12), and CO2-2× (experiment with CO<sub>2</sub> doubling). The three experiments were granted a sufficiently long spinup phase until a new climate equilibrium is reached, meaning that the surface temperature change has fully evolved. Compared to a deep ocean model, the MLO enables a relatively fast transition to the new climate state (Li et al. 2012). Only the subsequent phase of climate equilibrium was evaluated with respect to surface temperature changes and feedbacks. Note that the feedback analysis, when applied to the three MLO experiments, provides a combination of rapid radiative adjustments and slow feedbacks. To determine the slow feedbacks alone, the rapid radiative adjustments derived from the FSST simulations have been subtracted (Hodnebrog et al. 2020; Stecher et al. 2021). In total, 245 years of surface temperature change simulations were performed, of which 145 years are part of the climate equilibrium phases (cf. to Table 1).

TABLE 2. RFs derived with the EMAC–CCMod model, applying the FSST method. Two contrail cirrus simulations with different scalings of the underlying air traffic inventory (1× and 12×) and two CO<sub>2</sub> simulations were performed (+56 and +348 ppm). The CO<sub>2</sub> concentration of CO2-12 was chosen so that the corresponding classical RF approximately matches the classical RF of ATR-12 in order to enable a fair comparison of both simulations. Values in parentheses show the statistical uncertainties expressed by confidence intervals of the mean (conf) or standard deviations of the year-to-year variability. A comparison with the previously calculated RFs, derived with ECHAM5–CCMod, is shown in the supplemental material (see Table S1).

Name	CO <sub>2</sub> (ppmv)	Air traffic scaling	RF (conf) (W m <sup>-2</sup> )	ERF (conf) (W m <sup>-2</sup> )	ERF/RF (std dev)	Normalized ERF/RF (std dev)
ATR-1	348	1×	0.188 (±0.003)			
ATR-12	348	12×	0.858 (±0.004)	0.568 (±0.125)	0.66 (±0.34)	0.55 (±0.32)
CO2-12	404 (+56)	0×	0.854 (±0.001)	1.034 (±0.105)	1.21 (±0.32)	
CO2-2×	696 (+348)	0×	4.177 (±0.001)	4.574 (±0.094)	1.10 (±0.06)	

### 3. Results

#### a. Radiative forcings: Classical RF and ERF

The radiative forcing values resulting from the scaled simulations form the basis for our calculations of feedback and response parameters and will be presented in this subsection. We recall (see introduction) that the radiative forcing results from ATR-12 are not—and must not be—used to compute actual RFs and ERFs for 2050. As shown in Bickel et al. (2020, see their Figs. 1 and 3b), the radiative forcing parameters grow nonlinearly (less than the scaling factor), due to saturation effects related to the potential contrail cover in a model grid box (e.g., Bock and Burkhardt 2019) and limited availability of supersaturated water vapor for supplying a large number of contrails (e.g., Unterstrasser and Sölch 2013).

The ATR-12 FSST simulation yields a classical radiative forcing of 858 mW m<sup>-2</sup> (see Table 2). As explained above, it is advisable to carry out the comparison between contrail cirrus and a CO<sub>2</sub> perturbation with respect to rapid radiative adjustments, feedbacks, and the climate sensitivity on the basis of simulations, where the underlying classical RF of both forcers is similar in magnitude. The respective CO<sub>2</sub> experiment with +56 ppmv CO<sub>2</sub> (CO2-12) yields a classical RF of 854 mW m<sup>-2</sup> and fulfills this requirement almost perfectly. The corresponding ERF of the contrail cirrus experiment yields 568 mW m<sup>-2</sup>. Thus, the ERF is again lower than the classical RF for contrail cirrus (reduced to 66%), but the ERF reduction turns out to be weaker than in the corresponding, previously performed, simulations with ECHAM5–CCMod, where the ERF has decreased to 37% (Bickel et al. 2020, see Table 1 therein). An entire comparison of RF results derived with ECHAM5–CCMod and EMAC–CCMod can be found in the supplement to this paper (see Table S1 in the online supplemental material). For CO2-12, an ERF of 1034 mW m<sup>-2</sup> is obtained and is, therefore, larger than the corresponding classical RF (+21%). In contrast, the ECHAM5–CCMod simulations resulted in an ERF reduction of −11% for CO2-12. The origin of this difference will be discussed in the next subsection. The CO<sub>2</sub>-doubling experiment yielded a classical RF of 4177 mW m<sup>-2</sup> and an ERF of 4574 mW m<sup>-2</sup>, confirming the ERF increase for CO2-12 in EMAC–CCMod (but again deviating from the CO2-2× simulation with ECHAM5–CCMod reported in Bickel et al. 2020).

As mentioned, the contrail cirrus ERF/RF factor derived here (0.66) is substantially larger than that calculated with ECHAM5–CCMod (0.37). However, it has to be noted that the physically most meaningful question is, how much the ERF for contrail cirrus and CO<sub>2</sub> differs in case that both forcing agents exert the same classical RF? This difference is described by the ERF/RF factor only, if the classical RF and ERF are equal for CO<sub>2</sub>, an assumption implicitly made by Lee et al. (2021, see their Fig. 3) and supported by the multimodel mean evidence reported by Richardson et al. (2019). If this is not the case, the basic physical question (see above) is better described by a normalized ERF/RF factor, to be calculated as

$$\text{normalized ERF/RF factor} = \frac{\text{ERF}^{\text{ATR}}}{\text{RF}^{\text{ATR}}} \times \frac{\text{RF}^{\text{CO}_2}}{\text{ERF}^{\text{CO}_2}}. \quad (9)$$

When normalized, the ERF/RF factors of contrail cirrus agree considerably better between EMAC–CCMod (0.55) and ECHAM5–CCMod (0.42) and are close to the corresponding factor of 0.42 provided by Lee et al. (2021). We recall that the introduction of a correction factor  $\text{RF}^{\text{CO}_2}/\text{ERF}^{\text{CO}_2}$  is also required if the relation between the ERF/RF factor and the efficacy  $r$  is addressed (Lee et al. 2021; Ponater et al. 2021). The physically reasonable equation  $r_{\text{RF}}^{\text{ATR}} = \text{ERF}^{\text{ATR}}/\text{RF}^{\text{ATR}} \cdot r_{\text{RF}}^{\text{CO}_2}$  is only valid if the normalized  $\text{ERF}^{\text{ATR}}/\text{RF}^{\text{ATR}}$  factor is used (see section 2 of supplemental material).

#### b. Rapid radiative adjustments

Deviations of the ERF from the classical RF are a consequence of relatively fast adaptations of the atmosphere to the initial perturbation [Eq. (5)]. We determine the associated rapid RAs, separated into individual contributions, through a PRP feedback analysis (see section 2) of the FSST simulations. The results for the contrail cirrus experiment (ATR-12) are shown in Fig. 2. If all rapid RAs (left box) are summed up and added to the classical RF (middle box), the ERF (right box) is obtained. As clearly visible in the figure, the components most relevant in magnitude are the water vapor RA, the lapse-rate RA, and the natural cloud RA; other contributions remain negligible in ATR-12. Note that the water vapor as well as the lapse-rate RA are both dependent on temperature changes through the tropospheric vertical profile, and the associated RAs are known to largely compensate each other (e.g., for CO<sub>2</sub>, see Smith et al. 2018). For the contrail cirrus

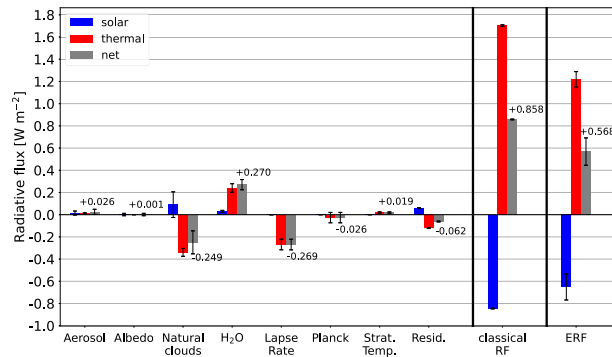


FIG. 2. Rapid RAs (left box) derived from the ATR-12 FSST simulation. The net radiative fluxes (gray bars) are subdivided into a shortwave part (blue bars) and longwave part (red bars). Whiskers represent the 95% confidence intervals of the mean based on the year-to-year variability. A comparison with the RAs derived in ECHAM5 of Bickel et al. (2020) is shown in the supplemental material (see Fig. S1).

case, this compensation is almost perfect. The natural cloud RA forms the largest individual RA contribution reducing the ERF. Indeed, with about  $-249 \text{ mW m}^{-2}$ , the natural cloud RA agrees relatively well with the ERF reduction of  $-290 \text{ mW m}^{-2}$ . An essential part of the natural cloud RA in reaction to the presence of contrail cirrus can be explained by the competition of natural and aviation-induced cirrus for water vapor supersaturation available for condensation (Burkhardt and Kärcher 2011; Bickel et al. 2020). An additional contribution may originate from upper troposphere stabilization causing cloud cover reduction, an effect known from other forcing mechanisms that induce peak heating near the tropopause (e.g., O'Connor et al. 2022). The vertical distribution of natural cirrus cover change showing up in the ATR-12 simulation with ECHAM5-CCMod (Bickel et al. 2020, their Fig. 5b) closely resembles the new one simulated by EMAC-CCMod (see Bickel 2023, his Fig. 4.6b).

In the CO<sub>2</sub>-12 FSST simulation, besides natural cloud, water vapor, and lapse-rate RA, also the Planck RA makes a significant contribution (see Fig. 3). The latter results from a slight surface warming over land areas (recall that only SSTs are prescribed), inducing a negative RA of similar magnitude as the lapse-rate RA. Despite of this, the ERF in CO<sub>2</sub>-12 is larger compared to the corresponding classical RF. This is mainly driven by a strongly positive natural cloud RA—in contrast to its respective negative contribution in ATR-12. A notable decrease in low-level (cooling) cloud coverage in CO<sub>2</sub>-12 is the origin of this feature, while in ATR-12, the decrease in (warming) natural cirrus cloud is dominating the natural cloud RA.

The compensation between positive water vapor RA and negative lapse-rate RA is not as complete in CO<sub>2</sub>-12 as in ATR-12, and a notable positive net RA remains for their sum (see Fig. 3), enhancing the ERF increase over the classical RF in CO<sub>2</sub>-12. This increased importance of the combined water vapor/lapse-rate feedback is confirmed by the (statistically more robust) feedback analysis of CO<sub>2</sub>-2 $\times$  (not shown). The

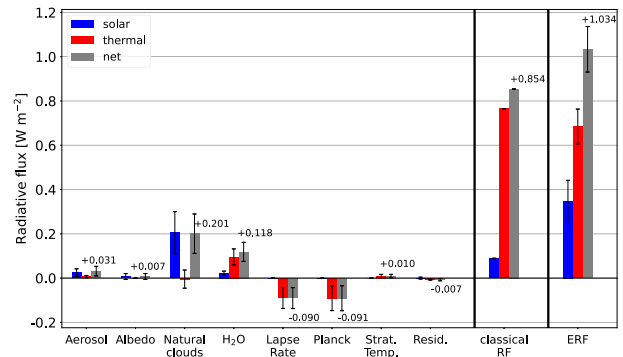


FIG. 3. As in Fig. 2, but for the CO<sub>2</sub>-12 FSST simulation. A comparison with the RAs derived in ECHAM5 of Bickel et al. (2020) is shown in the supplemental material (see Fig. S2).

more negative lapse-rate feedback in ATR-12 can likely be related to the contrail cirrus warming in the upper troposphere (Ponater et al. 2005; Schumann and Mayer 2017). The main driver of the different ERF/RF ratio between the two forcing mechanisms is the marked difference in the natural cloud RAs, just as in Bickel et al. (2020, see also Fig. S1). There is, however, a qualitative discrepancy of the natural cloud RA between the previous ECHAM5-CCMod CO<sub>2</sub> simulations (see Bickel et al. 2020, their Fig. 6b or Fig. S2), where the natural cloud RA was negative, while in the simulations reported here, it is positive (Fig. 3). This discrepancy also controls the quantitatively different ERF to the classical RF ratio in the two models. The difference may be found surprising as both models have so much in common, but it can be reconciled with the large variability that has been reported for the natural cloud RA of CO<sub>2</sub> in multimodel intercomparisons (e.g., Vial et al. 2013, see their Table 2, or Smith et al. 2018, see their Fig. 3 and Fig. S3). We note that the natural cloud RA of the model used here (EMAC-CCMod) is more in line with previously reported multimodel means (Vial et al. 2013; Smith et al. 2020). As pointed out in the previous subsection, a normalization of the contrail cirrus ERF/RF factor with the CO<sub>2</sub> ERF/RF factor [according to Eq. (9)] results in a better agreement of these factors between EMAC-CCMod and ECHAM5-CCMod. Starting from (by construction) similar classical RF values for contrail cirrus and CO<sub>2</sub>, the contrail cirrus ERF is reduced to about 55% of the CO<sub>2</sub> ERF in EMAC-CCMod and reduced to about 42% in ECHAM5-CCMod.

### c. Surface temperature change

To calculate the climate sensitivity parameters  $\lambda$  of contrail cirrus and CO<sub>2</sub> [Eqs. (1) and (4)], the changes in global mean surface temperature are needed. For this purpose, each FSST simulation was complemented by a corresponding counterpart using the model setup with coupled MLO (see Table 1). The resulting responses of global mean surface temperature change for the respective simulations are shown in Fig. 4. To fully relax the atmosphere toward the new sea surface temperature, when transitioning from FSST to MLO, the reference simulation (black line) of the MLO model was preceded by a 10-yr relaxation phase (see Fig. 4, year  $-10$  to  $0$ ). From

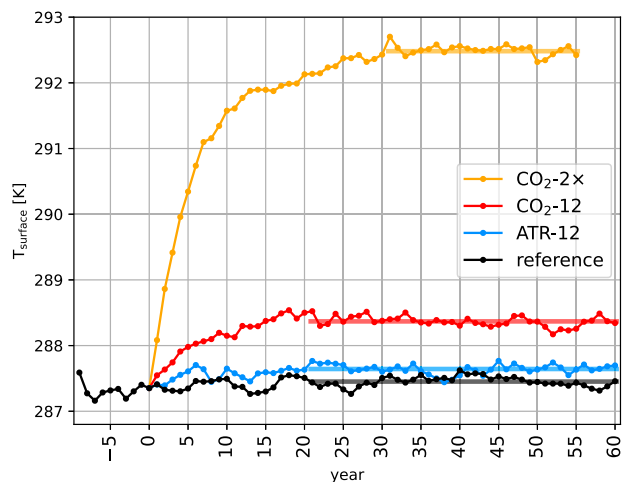


FIG. 4. Surface temperature changes induced by contrail cirrus (blue curve) and two different CO<sub>2</sub> increases (red and orange curves) derived from four EMAC–CCMod simulations with coupled MLO. The period up to year 0 was used as the relaxation phase for the unperturbed reference simulation (black curve). In year 0, the three experiments were branched off by adding the respective perturbations. Shaded horizontal lines show the mean temperatures of the respective periods, which mark the time frames where the simulations have restored equilibrium.

the following equilibrium reference state, three experiments were branched off, using the same perturbations as used for the FSST simulations: ATR-12 (blue line), CO<sub>2</sub>-12 (red line), and CO<sub>2</sub>-2× (orange line). The reference simulation, without perturbation, was continued to match the number of simulation years of the perturbation experiments. Following the branching off, the surface temperature of the experiments increases in reaction to the perturbed radiative balance. For the two experiments with smaller radiative forcing magnitude (ATR-12 and CO<sub>2</sub>-12), climate equilibrium is already restored after 20 years. In the CO<sub>2</sub>-doubling experiment (CO<sub>2</sub>-2×) with 5 times larger classical RF, the new equilibrium surface temperature is reached only after 30 years (note that the FSST simulations, where the freedom to move away from the initial state is limited by the prescribed lower boundary, only need a spinup phase of 3 years). The mean surface temperature increases derived from the equilibrium phases are illustrated by the shaded horizontal lines in Fig. 4. Note that the surface temperature development was not the only criterion to define the start of the analyzed equilibrium phases. Radiative quantities (e.g., radiative imbalance) and many other variables (e.g.,

snow and sea ice cover, precipitation, humidity) were also considered.

For ATR-12, a global mean surface temperature increase of +0.192 K was determined, which is small but statistically significantly different from zero on the 95% level (Table 3). However, the necessity of the aircraft inventory scaling is confirmed. For CO<sub>2</sub>-12, which features a similarly sized classical RF as ATR-12, a considerably larger surface temperature increase of +0.916 K is simulated, which is significantly different from both, zero and the ATR-12 response. Thus, if based on a similarly sized classical RF, the surface temperature increase induced by contrail cirrus is about 5 times smaller than for CO<sub>2</sub>. The CO<sub>2</sub>-doubling simulation features the largest surface temperature increase of about +5 K, posing no statistical detection problems at all (see Table 3) despite the shorter equilibrium phase of only 25 years.

#### d. Climate sensitivity and efficacy parameters

The climate sensitivity parameter  $\lambda$  provides the relation between radiative forcing and global surface temperature change for individual forcing mechanisms [see Eqs. (1) and (4)], while climate efficacy describes the relative change of this relation from the CO<sub>2</sub> reference case to a non-CO<sub>2</sub> forcer [see Eqs. (2) and (3)]. By combining the radiative forcings shown in Table 2 with the respective surface temperature changes presented in Table 3, both, climate sensitivity and efficacy parameter, can be determined (see also Table 3). Depending on the used RF framework (classical or effective RF), different climate sensitivity and efficacy values result (e.g., Richardson et al. 2019; Ponater et al. 2021).

Based on the ERF, a climate sensitivity parameter of 0.337 KW<sup>-1</sup> m<sup>2</sup> results for ATR-12. Relative to the climate sensitivity of CO<sub>2</sub>-12 (0.887 KW<sup>-1</sup> m<sup>2</sup>), an efficacy of 0.380 is yielded. As a consequence of the different ERF/RF ratios from ATR-12 and CO<sub>2</sub>-12 (see Table 2), the climate sensitivity parameter based on the classical RF is smaller for ATR-12 but larger for CO<sub>2</sub>-12 and CO<sub>2</sub>-2×. The effect of larger CO<sub>2</sub> perturbations leading to larger climate sensitivities is also visible (see Table 3), consistent with previous work (e.g., Hansen et al. 2005; Meraner et al. 2013; Rieger et al. 2017).

Straightforward derivation of the statistical uncertainty parameters [standard deviations (std devs) and confidence intervals] for the climate sensitivity parameters relies on the assumption that both, radiative forcings and surface temperature changes, are normally distributed, which proved to be the case for these parameters (see Bickel 2023, his Fig. 4.10). Dividing two normal distributions [viz., surface temperature change

TABLE 3. Surface temperature changes ( $\Delta T_{\text{surface}}$ ), climate sensitivity parameters ( $\lambda$ ), and efficacies ( $r$ ) derived from EMAC–CCMod simulations with FSST and coupled MLO. Contrail cirrus efficacy parameters use the CO<sub>2</sub>-12 simulation as reference. Values in parentheses show the statistical uncertainties expressed by one std dev of the year-to-year variability.

	ATR-12	CO <sub>2</sub> -12	CO <sub>2</sub> -2×
$\Delta T_{\text{surface}}$ (K)	+0.192 ( $\pm 0.106$ )	+0.916 ( $\pm 0.108$ )	+5.050 ( $\pm 0.096$ )
$\lambda_{\text{RF}}$ (KW <sup>-1</sup> m <sup>2</sup> )	0.223 ( $\pm 0.124$ )	1.073 ( $\pm 0.127$ )	1.209 ( $\pm 0.026$ )
$r_{\text{RF}}$	0.208 ( $\pm 0.106$ )		
$\lambda_{\text{ERF}}$ (KW <sup>-1</sup> m <sup>2</sup> )	0.337 ( $\pm 0.254$ )	0.887 ( $\pm 0.257$ )	1.104 ( $\pm 0.068$ )
$r_{\text{ERF}}$	0.380 ( $\pm 0.257$ )		

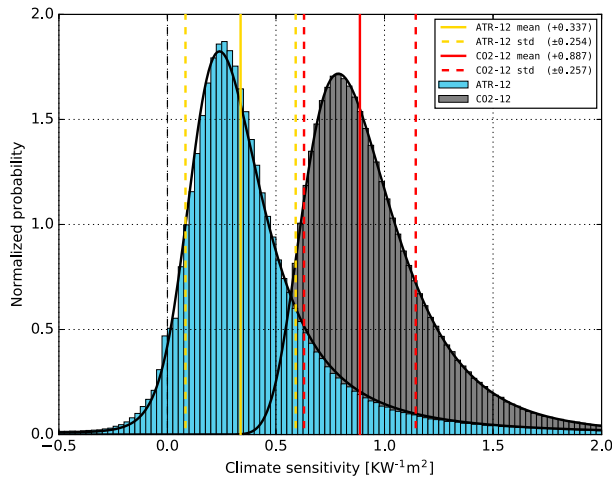


FIG. 5. Distribution of climate sensitivity parameters in the framework ERF  $\lambda_{\text{ERF}}$  for ATR-12 (blue) and CO2-12 (gray). Both climate sensitivity parameters follow ratio distributions (black curves). Mean values are illustrated by vertical solid lines, while vertical dashed lines indicate one standard deviation interval, based on the year-to-year variability.

and radiative forcing, following Eqs. (1) and (4)] results in a so-called ratio distribution. The standard deviations for this ratio distribution of the climate sensitivity parameter were derived following Díaz-Francés and Rubio (2013, see their Eq. (8) and are about 2 times larger in the ERF framework, as the ERF features a substantially higher statistical uncertainty compared to the classical RF [see Table 2, or Bickel et al. (2020), their Fig. 1]. Nevertheless, the ERF-based climate sensitivity parameter of ATR-12 is significantly different from that of CO2-12 as well as from zero (see dashed vertical lines in Fig. 5). We note that the distributions of climate sensitivities are obtained from a bootstrap analysis through combining all annual mean radiative forcings with all annual mean surface temperature change values from the equilibrium phases. It should also be mentioned that the mean of the distribution is slightly larger than the maximum probability (mode value), resulting from the common skewness of the ratio distribution.

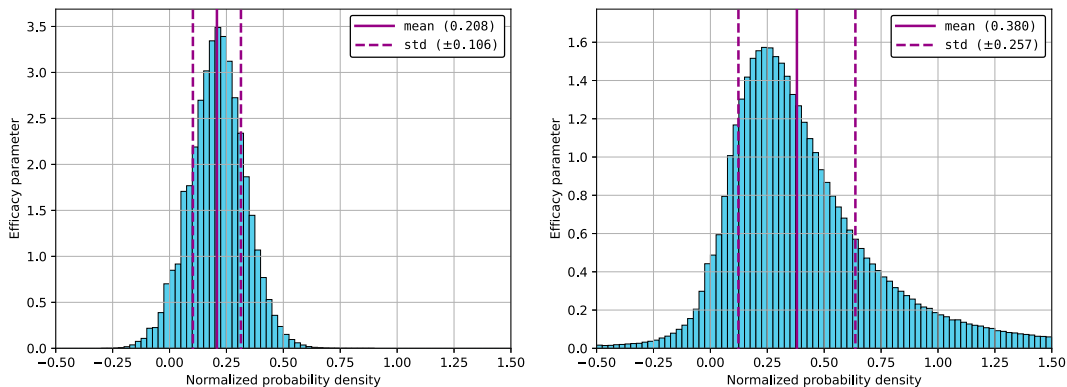


FIG. 6. Distribution of contrail cirrus efficacy parameters based on the (left) classical RF and (right) ERF, derived by dividing the climate sensitivity parameters from ATR-12 by those from CO2-12. The statistical uncertainty is illustrated by the standard deviation on the basis of internal interannual variabilities.

Figure 6 shows the distribution of the contrail cirrus efficacy based on the classical RF (left) and ERF (right). The distribution is obtained by performing a bootstrap analysis of the climate sensitivities derived from the ATR-12 and CO2-12 simulations. The determination of statistical parameters for the efficacy entails a quotient of two ratio distributions, which is not easy to treat analytically. The whiskers in Fig. 6 represent the standard deviations based on the interannual variability calculated after the rules of error propagation. Note that the width of the classical RF-based efficacy distribution (left panel of Fig. 6) is considerably narrower due to its underlying uncertainty being much smaller than for the ERF. Nevertheless, both distributions indicate that the efficacy of contrail cirrus to warm Earth's surface is very likely smaller than one and very unlikely to be negative.

#### e. Slow feedbacks and feedback parameters

To physically understand the low climate efficacy of contrail cirrus, the PRP feedback analysis was applied to ATR-12 and CO2-12 results to derive the slow feedbacks. Following Eq. (7), the slow feedbacks, when normalized by the corresponding surface temperature change to obtain the feedback parameters, are directly comparable between both simulations. In Fig. 7, the respective feedback parameters of ATR-12 are compared to those of CO2-12. Feedback parameters are in close agreement for the aerosol, albedo, water vapor, Planck, and stratospheric temperature feedback. We mention that the warming induced by contrail cirrus hardly feeds back on the contrail cirrus itself (see Bickel 2023, his Figs. 4.13 and 4.14b). This is consistent with previous studies that indicated a small sensitivity of contrails to moderate background warming (Marquart et al. 2003; Chen and Gettelman 2016; Bock and Burkhardt 2019). However, differences between ATR-12 and CO2-12 are considerably larger for the lapse-rate and natural cloud feedback parameters, and in the latter case, even the sign changes.

The large difference in the cloud feedback parameter can be mainly attributed to a different reaction of the low- and midlevel cloud cover in both simulations, which is substantially decreasing in CO2-12 at almost all latitudes (see Fig. 8c,

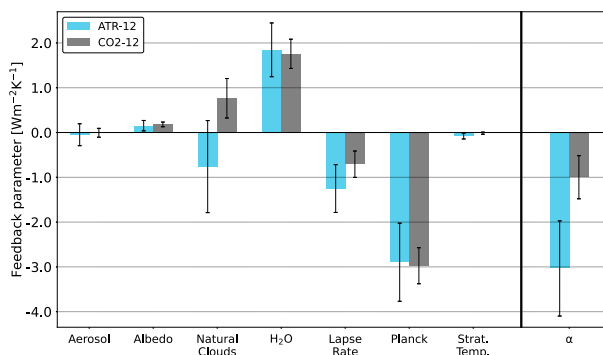


FIG. 7. Comparison of FPs derived for contrail cirrus (blue) and CO<sub>2</sub> (gray). The total feedback parameter  $\alpha$  corresponds to the negative inverse of the climate sensitivity in  $\lambda_{\text{ERF}}$ . Whiskers depict the year-to-year standard deviation.

illustrated for CO<sub>2</sub>-2 $\times$ , which shows a qualitatively similar response as CO<sub>2</sub>-12), but possibly slightly increasing for ATR-12 (not shown here, as the changes are mostly statistically insignificant). Hence, when globally averaged, the absolute natural cloud slow feedback is strongly positive and the corresponding feedback parameter is significantly positive for CO<sub>2</sub>-12, while for contrail cirrus, the respective feedback parameter is more likely negative than positive. When normalized with the (small) surface temperature change in ATR-12, the cloud feedback parameter is similar in magnitude but more noisy for ATR-12 (see Fig. 7). The larger lapse-rate feedback parameter in case of ATR-12 can be attributed to more distinct warming of the upper troposphere in the contrail case, over almost all latitudes south of 70°N (see Figs. 8a,b). This is consistent with the contrail cirrus known to provide strongest instantaneous radiative heating directly below the cloud base (e.g., Schumann and Mayer 2017; Ponater et al. 2021). In contrast, the CO<sub>2</sub>-induced warming is distributed more homogeneously throughout the whole depth of the troposphere (e.g., Clough and Iacono 1995).

Thus, because in ATR-12 two feedbacks either become more negative (lapse-rate) or negative rather than positive

(natural clouds) in comparison to CO<sub>2</sub>-12, the total feedback parameter  $\alpha$  is significantly more negative (right column in Fig. 7) for contrail cirrus than for CO<sub>2</sub>. This explains the smaller climate sensitivity parameter ( $\lambda_{\text{ERF}}$ ), which is the negative inverse of the feedback parameter [see Eq. (8)].

#### 4. Discussion and conclusions

Based on global climate model simulations including a parameterization of contrail cirrus (ECHAM5-CCMod), Bickel et al. (2020) concluded that the ERF of contrail cirrus is reduced to about 37% with respect to its classical RF, while our current study estimates the contrail cirrus ERF to be reduced to 66%. According to the current radiative forcing concept (Ramaswamy et al. 2018), the efficacy of any perturbation to induce surface temperature changes is well described by the ERF/RF factor, which means that a nearly constant climate sensitivity parameter is valid for all perturbations. Thus, the assessment paper of Lee et al. (2021) has ranked the relevance of the various climate effect components of global aviation preferentially by their respective ERF, which implies that the effect of contrail cirrus still makes the largest contribution—though not as distinct as the classical RF would have suggested. The present study now provides a consistent set of classical and effective radiative forcing, feedback, and climate sensitivity parameters, as well as directly simulated surface temperature response results. They are obtained with the same contrail cirrus parameterization (Bock and Burkhardt 2016a) as used by Bickel et al. (2020; ECHAM5-CCMod), but now in a slightly modified host climate model (EMAC-CCMod). It is found that the simulated global mean surface temperature change and, thus, the efficacy of contrail cirrus are even more reduced than the ERF/RF ratio suggests. If the contrail cirrus and the CO<sub>2</sub> increase exert the same classical radiative forcing, the contrail cirrus ERF is about 55% of the CO<sub>2</sub> ERF (in ECHAM5-CCMod, the respective value was 42%). However, the global mean equilibrium surface temperature increase induced by the contrail cirrus classical RF (i.e., the efficacy) is as low as 21% when compared to the respective CO<sub>2</sub>-forced response. This means that the efficacy of contrail cirrus to drive surface temperature changes is smaller

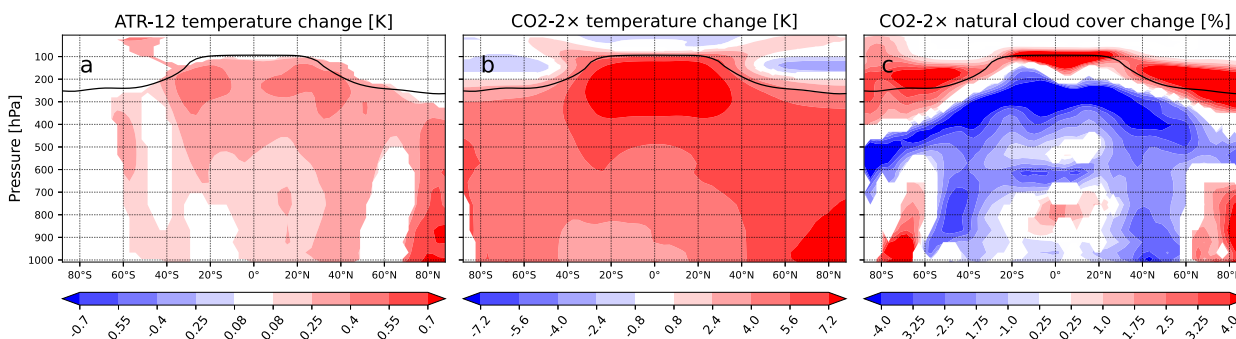


FIG. 8. Zonal mean vertical cross section of temperature change for (a) ATR-12 and (b) CO<sub>2</sub>-2 $\times$  and (c) natural cloud cover change of CO<sub>2</sub>-2 $\times$  as a reaction to surface temperature change. As for the feedback parameters (see Fig. 7), the rapid adjustments of temperature and cloud cover have been subtracted from the full response in the MLO simulations. The black solid line shows the climatological tropopause height of the reference simulation. Changes are only plotted where significant at the 99% confidence level with respect to the interannual variability.

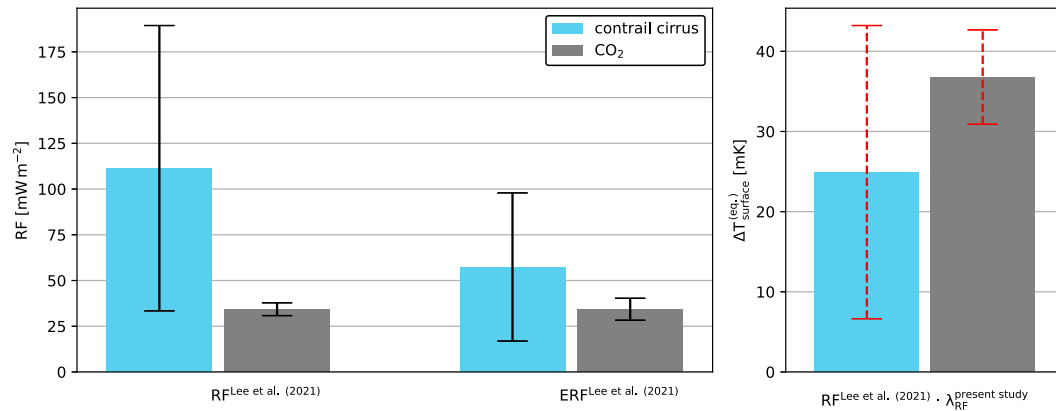


FIG. 9. (right) Estimation of the contrail cirrus climate impact on global surface temperature, derived by multiplying the (left) classical RF of Lee et al. (2021) for the year 2018 with the respective climate sensitivity parameter of the present study. Whiskers of RF and ERF show the 5%–95% confidence interval of the RF taken from Lee et al. (2021), see their Fig. 3) and were derived partly by expert judgment therein [see appendix E of Lee et al. (2021)]. Whiskers of the surface temperature change (red dashed) were estimated by combining Lee et al.’s (2021) RF systematic uncertainty with the statistical variability derived for the respective climate sensitivity parameter of the present work.

than for any of the various forcing agents tested by Richardson et al. (2019) within the CMIP6 framework. Our results are qualitatively consistent with the evidence of an efficacy much below unity for line-shaped contrails, as reported in earlier studies (Ponater et al. 2005; Rap et al. 2010; Ponater 2010). The efficacy value for contrail cirrus, as indicated by the present study, is even lower. It might, on the one hand, be regarded as more credible because the CCMod parameterization involves a more realistic coupling for contrail cirrus ice water to the hydrological cycle, which considers the contrail cirrus ice crystal growth at the expense of ambient water vapor over the whole life time of a contrail cirrus cluster (Bock and Burkhardt 2016a). On the other hand, we have to keep in mind that the contrail cirrus efficacy also depends on the CO<sub>2</sub> climate sensitivity, which has been known for its large intermodel dependency related to systematic uncertainties in the cloud radiative feedback (e.g., Andrews et al. 2012; Zelinka et al. 2020; Bock and Lauer 2024). A respective knowledge on systematic uncertainties in contrail cirrus feedbacks is currently nonexistent, however.

For our EMAC–CCMod simulations, contrail cirrus and CO<sub>2</sub> classical RFs have been scaled to the same magnitude, in order to make the resulting climate sensitivity and feedback parameters optimally comparable. The magnitudes of the radiative forcings are far larger than those given by Lee et al. (2021) for present-day (year 2018) conditions—a necessary scaling to limit the statistical uncertainty of the directly simulated climate parameters (ERF/RF ratio, radiative feedbacks, surface temperature change, and efficacy). However, it is possible to combine the present-day aviation radiative forcings provided by Lee et al. (2021, their Tables 2 and 3), including the associated model and parameter uncertainties [partly yielded via expert judgment in Lee et al. (2021), see their appendix E], with the climate sensitivity parameters derived within the present study, including their associated statistical uncertainties (see Table 3 and Fig. 5). This is possible because

the climate sensitivity difference between two climate forcings (and, thus, their efficacy) is assumed to be largely constant in time [Fuglestedt et al. 2003, their Eq. (7)], being controlled by specific feedbacks characteristic for these forcings (e.g., Stuber et al. 2005; Kaur et al. 2023; Zhou et al. 2023; Aeronson et al. 2024). Utilizing this feature, it can be illustrated how the relative importance of the contrail cirrus and aviation CO<sub>2</sub> increase contributions to global aircraft climate impact changes, on the way from conventional radiative forcing, over effective radiative forcing, to global surface warming (Fig. 1). While, for 2018, the radiative forcing best estimates of contrail cirrus are larger than for aviation CO<sub>2</sub> by a factor of about 3.2 (for classical RF) or of about 1.7 (for ERF), the same relative factor drops to about 0.65 for the equilibrium global surface temperature change (Fig. 9). This challenges the notion of a leading role of contrail cirrus in forcing aviation “climate impact,” which has been repeatedly expressed in recent literature. We emphasize that the efficacy parameter is not only of relevance for equilibrium temperature change but also affects results from advanced temperature targeted metrics like the global temperature potential (GTP) (e.g., Fuglestedt et al. 2003, 2010; Lund et al. 2017) as well as from linear response models describing the transient development of global surface temperature change in response to certain future aviation emission scenarios (e.g., Ponater et al. 2006; Dallara et al. 2011; Grewe et al. 2021; Megill et al. 2024). Global warming potentials (e.g., Lee et al. 2021, their Table 5) are also suitable to account for the efficacy effect [Borella et al. 2024; Fuglestedt et al. 2003, their Eq. (7)].

Previous assessments of the aviation climate impact have frequently retained the use of an efficacy of 1 for all radiative forcing agents (e.g., Marais et al. 2008; Fuglestedt et al. 2008; Lund et al. 2017; Klöwer et al. 2021). This decision was made, partly, because of a lack of physical understanding and no climate model consensus on efficacy parameters deviating from unity, but in recent years also because the efficacy issue

appeared to have been superseded by using the revised, ERF-based, radiative forcing concept (Myhre et al. 2013; Ramaswamy et al. 2018; Richardson et al. 2019; Lee et al. 2021). Because of the low efficacy of contrail cirrus (0.38) even within the ERF framework, as found in this study, we urgently recommend to account for the efficacy parameter estimates in future assessments of aviation-induced global warming, e.g., with regard to the Paris Agreement (Grewe et al. 2021; Fuglestedt et al. 2023). As a minimum, the sensitivity of such assessments to the inclusion or omission of efficacies should be tested.

To identify physical reasons for a varying efficacy among forcing mechanisms, many previous papers have profited from the application of a complete analysis of feedbacks (Yoshimori and Broccoli 2008; Rieger et al. 2017; Richardson et al. 2019; Kaur et al. 2023), and this method proved to be beneficial here as well. It is essential to note the existence of several almost independent physical mechanisms, which all contribute to low contrail cirrus efficacy by dampening its surface temperature response. The competition of contrail cirrus and natural cirrus for ice supersaturated water vapor available for condensation has already been discussed by Burkhardt and Kärcher (2011) and Bickel et al. (2020). It appeared to be the main reason for a negative cloud rapid radiative adjustment in ECHAM5-CCMod, reducing the ERF of contrail cirrus more strongly than in the CO<sub>2</sub> case. This mechanism is also apparent in the EMAC-CCMod model applied here, with even a different sign of the natural cloud adjustment between both forcing types. A secondary effect, which also contributes to a smaller ERF/RF factor in the contrail cirrus case, is related to the characteristic pattern of contrail cirrus-induced local radiative heating. It peaks near the tropopause region, close to the edge of the convectively mixed domain. This may indicate a reduction of downward transport of the warming signal (Forster et al. 1997; Schumann and Mayer 2017), thus providing a direct influence on the lapse rate. While in the case of CO<sub>2</sub>-induced warming, a rather stable anticorrelation between water vapor and lapse-rate rapid adjustment exists at extratropical latitudes (Colman and Soden 2021), and for the contrail case, the balance is tipped toward a less positive combined water vapor and lapse-rate adjustment.

The analysis of slow feedback parameters (Fig. 7) also indicates that the lapse-rate and natural cloud slow feedbacks make the main contributions to contrail cirrus efficacy reduction. However, closer inspection reveals that the physical mechanisms are quite different from those controlling the respective rapid adjustments. The lapse-rate feedback receives both negative and positive contributions to its global mean, depending on latitude, but the transition from negative to positive values occurs at different latitudes in the contrail cirrus and the CO<sub>2</sub> case (not shown here). In the latter case, the sign changes at midlatitudes (between 45° and 50°N), consistent with literature (Bitz et al. 2012; Chung and Soden 2015b; Colman and Hanson 2017), while for contrail cirrus, a positive lapse-rate feedback is limited to latitudes poleward of 60°N, making the global combined water vapor/lapse-rate feedback less positive than for CO<sub>2</sub>. Quantitatively more important, however, is the contribution of the natural cloud feedback,

which emerges positive in the CO<sub>2</sub> case but negative in the contrail cirrus case. As shown in the results section (see Fig. 8), this difference mainly originates from the response (coverage decrease) of low clouds in the CO<sub>2</sub> simulations, which provides a positive cloud radiative feedback. We note that a positive cloud feedback parameter is consistent with what has been reported in CMIP-related comparisons of CO<sub>2</sub> increase simulations (Ceppi et al. 2017; Sherwood et al. 2020, their Figs. 1 and 7, respectively), but the corresponding value of about 0.75 W m<sup>-2</sup> K<sup>-1</sup>, as found in the EMAC-CCMod model, is relatively high (though still within the multimodel range reported in the CMIP studies). In the contrail cirrus simulations, the natural cloud slow feedback, albeit rather noisy, has a high probability of being negative rather than positive. There is no clear signal of a large-scale low cloud decrease here, rather there are indications of low cloud increases at northern polar latitudes and high cloud decreases at tropical latitudes. Limited statistical significance in the contrail case, however, does not allow a straightforward attribution of the negative cloud feedback to a controlling individual physical process.

As pointed out by Bickel et al. (2020, their Fig. 3), upscaling the aircraft inventory modifies the zonal structure of the contrail cirrus RF. This could limit the validity of conclusions drawn from scaled simulations (like ATR-12) for the unscaled case, because certain interaction and feedback processes may work differently at different geographical latitudes. The natural cloud rapid adjustment, essential for the low ERF/RF ratio in the contrail cirrus case, has been shown to be rather robust to different scaling factors (Bickel et al. 2020; Ponater et al. 2021). The differences in the natural cloud slow feedback between the contrail cirrus and CO<sub>2</sub> case are mainly a result of a low cloud response missing in the contrail case, a feature that is unlikely to be affected by the contrail scaling procedure (for more details see section 3 of the supplemental material).

## 5. Outlook

Accounting for efficacies that deviate strongly from unity is very important when assessing the usefulness of a mitigation measure that involves additional fuel consumption, as has been demonstrated for the case of contrail avoidance by flying lower (Deuber et al. 2013; Irvine et al. 2014) or deliberate avoidance of contrail susceptible airspace (Borella et al. 2024). Nevertheless, due to methodical reasons (e.g., statistical accuracy, comparability to observations), for a local quantification of the contrail cirrus radiative effect, the classical radiative forcing will remain the first choice, for example, to characterize its distinctive day–night impact (Stuber et al. 2006; Newinger and Burkhardt 2012; Schumann and Graf 2013) or to assess individual flights (e.g., Schumann et al. 2012; Teoh et al. 2020b; Yamashita et al. 2020; Dahmann et al. 2023). The same holds for regional evaluation of the contrail radiative effect with observations, as has been done for, e.g., the period of reduced aviation activity during the COVID-19 period (Gettelman et al. 2021; Quaas et al. 2021; Schumann et al. 2021; Duda et al. 2023). We cannot recommend “correcting” local classical RFs using the global ERF/RF or efficacy parameter as an

improvement. The spatial correlation of the classical RF and expected climatological surface temperature change is known to be weak (e.g., Boer and Yu 2003; Shindell et al. 2015) because rapid adjustments and slow feedbacks modify the RF geographical distributions through their own characteristic spatial patterns (Vial et al. 2013; Chung and Soden 2015b; Smith et al. 2020). Hence, there is no such thing like a local climate sensitivity parameter with the same value for all regions or seasons (Shine 2015; Ramaswamy et al. 2018; Lee et al. 2023) that would allow to upgrade the usefulness of the RF on the local scale. If, however, the mitigation potential of a multitude of flights is evaluated based on local RF trade-off considerations (e.g., Teoh et al. 2020b), then it is indispensable to account for the efficacy factor in order to assess whether, in total, a limitation of aviation-induced global warming will actually be achieved (Teoh et al. 2020a; Borella et al. 2024).

Differences between climate sensitivity parameters for individual forcings can hardly be evaluated with observations. Yet, by revealing differences in several (rapid as well as surface temperature driven) global feedbacks between contrail cirrus and CO<sub>2</sub>, our study opens a perspective for a targeted search for key processes that trigger the low contrail cirrus climate sensitivity.

However, global feedback parameters are known to vary considerably between different climate models (e.g., Andrews et al. 2012; Vial et al. 2013; Smith et al. 2018; Richardson et al. 2019). The results from this study, regarding radiative adjustments and feedbacks that are specific for contrail cirrus forcing, therefore, need support from other independent global models. This is emphasized by the fact that for the ERF/RF factor, some noticeable differences have been pointed out between ECHAM5-CCMod and EMAC-CCMod, despite the close kinship of both models. The robustness of key feedback parameters needs to be consolidated and confirmed by other global models, while the processes controlling these feedbacks may be evaluated by process modeling or dedicated observational studies. This holds, in particular, for the competition of contrail cirrus and natural cirrus for available supersaturated water vapor (Heymsfield et al. 2010; Lewellen et al. 2014; Unterstrasser et al. 2017; Verma and Burkhardt 2022). The positive radiative feedback from low clouds in the CO<sub>2</sub> case (Fig. 7) also plays a crucial role for the low contrail cirrus efficacy, as this feedback does not show up in the contrail cirrus case. The magnitude of that feedback has been under close scrutiny for quite some time but still has remained controversial (e.g., Schneider et al. 2019; Zelinka et al. 2020; Ceppi and Nowack 2021; McCoy et al. 2022; Vogel et al. 2022). Thus, progress and consolidation in the research field of natural cloud feedbacks will also make an important contribution to increase the confidence in contrail cirrus efficacy estimates.

To simulate statistically significant feedback and response results for contrail cirrus, without scaling the contrail forcing, the only promising option is the use of the nudging technique as demonstrated by, e.g., Chen and Gettelman (2013). Increasing the signal-to-noise ratio would also help to identify significant regional contributions to the global feedbacks. The nudging method has already been applied within the EMAC model in various configurations (e.g., Jöckel et al. 2016; Righi

et al. 2021, 2023). As mentioned in section 2, ensuring the equivalence of adjustments and feedbacks in nudged and free-running model simulations, respectively, will require some preparatory work. For proceeding along this path in future studies, the present model appears to be well suited.

Remaining uncertainties related to contrail cirrus microphysics representation have been discussed by Bier and Burkhardt (2022, their section 7.2), and as one step forward, a refinement of the ice nucleation parameterization was utilized in their simulations. For a thorough improvement of the dynamics associated with natural cloud and contrail cirrus formation, it is desirable to forward development and application of cloud resolving models (Stevens et al. 2019, 2020), though it will take some time before such models will be available for multidecadal simulations on the global scale. Other model biases like the notorious upper troposphere cold bias in global models (Roeckner et al. 2006; Jöckel et al. 2016) do also represent potential for improving the basis of contrail cirrus radiative impact studies. Such progress, however, will mainly help to make model-simulated microphysical and macrophysical contrail cirrus properties more realistic and more suitable for comparison with observations. Yet, this should not distract from the central message of the present paper: For a reliable estimate of the contrail cirrus global climate impact, a good representation of microphysical processes and properties alone (though doubtless fundamental) is not sufficient, but the global feedbacks induced are of comparable importance and deserve more attention than they have hitherto received.

*Acknowledgments.* We sincerely thank Robert Sausen (DLR) and Klaus Gierens (DLR) for their essential contributions to the statistical analyses. Our gratitude also extends to Simone Dietmüller (DLR), Axel Lauer (DLR), and the three anonymous reviewers for their thoughtful critiques and detailed feedbacks. We gratefully acknowledge the German Climate Computing Center (DKRZ) for providing the computational resources necessary for this work. This work received dedicated funding from the DLR Aeronautics Board under the Ph.D. project “Efficacy of Contrail Cirrus.” A large portion of this paper is derived from the first author’s Ph.D. thesis, supervised by Robert Sausen, to whose memory the authors dedicate this publication.

*Data availability statement.* All data used in this study are available upon request.

## REFERENCES

- Aerenson, T., R. Marchand, and C. Zhou, 2024: Cloud responses to abrupt solar and CO<sub>2</sub> forcing: 2. Adjustment to forcing in coupled models. *J. Geophys. Res. Atmos.*, **129**, e2023JD040297, <https://doi.org/10.1029/2023JD040297>.
- Andrews, T., J. M. Gregory, M. J. Webb, and K. E. Taylor, 2012: Forcing, feedbacks and climate sensitivity in CMIP5 coupled atmosphere-ocean climate models. *Geophys. Res. Lett.*, **39**, L09712, <https://doi.org/10.1029/2012GL051607>.
- Bickel, M., 2023: Climate impact of contrail cirrus. Ph.D. dissertation, Ludwig-Maximilians-Universität München, 154 pp., <https://doi.org/10.5282/edoc.32411>.

- , M. Ponater, L. Bock, U. Burkhardt, and S. Reineke, 2020: Estimating the effective radiative forcing of contrail cirrus. *J. Climate*, **33**, 1991–2005, <https://doi.org/10.1175/JCLI-D-19-0467.1>.
- Bier, A., and U. Burkhardt, 2019: Variability in contrail ice nucleation and its dependence on soot number emissions. *J. Geophys. Res. Atmos.*, **124**, 3384–3400, <https://doi.org/10.1029/2018JD029155>.
- , and —, 2022: Impact of parametrizing microphysical processes in the jet and vortex phase on contrail cirrus properties and radiative forcing. *J. Geophys. Res. Atmos.*, **127**, e2022JD036677, <https://doi.org/10.1029/2022JD036677>.
- Bitz, C. M., K. M. Shell, P. R. Gent, D. A. Bailey, G. Danabasoglu, K. C. Armour, M. M. Holland, and J. T. Kiehl, 2012: Climate sensitivity of the Community Climate System Model, version 4. *J. Climate*, **25**, 3053–3070, <https://doi.org/10.1175/JCLI-D-11-00290.1>.
- Bock, L., 2014: Modellierung von Kondensstreifenzirren: Mikrophysikalische und optische Eigenschaften. Ph.D. dissertation, Ludwig-Maximilians-Universität München, 111 pp., <https://doi.org/10.5282/edoc.17026>.
- , and U. Burkhardt, 2016a: The temporal evolution of a long-lived contrail cirrus cluster: Simulations with a global climate model. *J. Geophys. Res. Atmos.*, **121**, 3548–3565, <https://doi.org/10.1002/2015JD024475>.
- , and —, 2016b: Reassessing properties and radiative forcing of contrail cirrus using a climate model. *J. Geophys. Res. Atmos.*, **121**, 9717–9736, <https://doi.org/10.1002/2016JD025112>.
- , and —, 2019: Contrail cirrus radiative forcing for future air traffic. *Atmos. Chem. Phys.*, **19**, 8163–8174, <https://doi.org/10.5194/acp-19-8163-2019>.
- , and A. Lauer, 2024: Cloud properties and their projected changes in CMIP models with low to high climate sensitivity. *Atmos. Chem. Phys.*, **24**, 1587–1605, <https://doi.org/10.5194/acp-24-1587-2024>.
- Boer, G. J., and B. Yu, 2003: Climate sensitivity and response. *Climate Dyn.*, **20**, 415–429, <https://doi.org/10.1007/s00382-002-0283-3>.
- Borella, A., O. Boucher, K. P. Shine, M. Stettler, K. Tanaka, R. Teoh, and N. Bellouin, 2024: The importance of an informed choice of CO<sub>2</sub>-equivalence metrics for contrail avoidance. *Atmos. Chem. Phys.*, **24**, 9401–9417, <https://doi.org/10.5194/acp-24-9401-2024>.
- Boucher, O., 2011: Seeing through contrails. *Nat. Climate Change*, **1**, 24–25, <https://doi.org/10.1038/nclimate1078>.
- Brasseur, G. P., and Coauthors, 2016: Impact of aviation on climate: FAA's Aviation Climate Change Research Initiative (ACCRI) phase II. *Bull. Amer. Meteor. Soc.*, **97**, 561–583, <https://doi.org/10.1175/BAMS-D-13-00089.1>.
- Burkhardt, U., and B. Kärcher, 2009: Process-based simulation of contrail cirrus in a global climate model. *J. Geophys. Res.*, **114**, D16201, <https://doi.org/10.1029/2008JD011491>.
- , and —, 2011: Global radiative forcing from contrail cirrus. *Nat. Climate Change*, **1**, 54–58, <https://doi.org/10.1038/nclimate1068>.
- Ceppi, P., and P. Nowack, 2021: Observational evidence that cloud feedback amplifies global warming. *Proc. Natl. Acad. Sci. USA*, **118**, e2026290118, <https://doi.org/10.1073/pnas.2026290118>.
- , F. Brient, M. D. Zelinka, and D. L. Hartmann, 2017: Cloud feedback mechanisms and their representation in global climate models. *Wiley Interdiscip. Rev.: Climate Change*, **8**, e465, <https://doi.org/10.1002/wcc.465>.
- Chen, C.-C., and A. Gettelman, 2013: Simulated radiative forcing from contrails and contrail cirrus. *Atmos. Chem. Phys.*, **13**, 12 525–12 536, <https://doi.org/10.5194/acp-13-12525-2013>.
- , and —, 2016: Simulated 2050 aviation radiative forcing from contrails and aerosols. *Atmos. Chem. Phys.*, **16**, 7317–7333, <https://doi.org/10.5194/acp-16-7317-2016>.
- Chung, E.-S., and B. J. Soden, 2015a: An assessment of methods for computing radiative forcing in climate models. *Environ. Res. Lett.*, **10**, 074004, <https://doi.org/10.1088/1748-9326/10/7/074004>.
- , and —, 2015b: An assessment of direct radiative forcing, radiative adjustments, and radiative feedbacks in coupled ocean–atmosphere models. *J. Climate*, **28**, 4152–4170, <https://doi.org/10.1175/JCLI-D-14-00436.1>.
- Clough, S. A., and M. J. Iacono, 1995: Line-by-line calculation of atmospheric fluxes and cooling rates: 2. Application to carbon dioxide, ozone, methane, nitrous oxide and the halocarbons. *J. Geophys. Res.*, **100**, 16 519–16 535, <https://doi.org/10.1029/95JD01386>.
- Colman, R., and B. J. McAvaney, 1997: A study of general circulation model climate feedbacks determined from perturbed sea surface temperature experiments. *J. Geophys. Res.*, **102**, 19 383–19 402, <https://doi.org/10.1029/97JD00206>.
- , and L. Hanson, 2017: On the relative strength of radiative feedbacks under climate variability and change. *Climate Dyn.*, **49**, 2115–2129, <https://doi.org/10.1007/s00382-016-3441-8>.
- , and B. J. Soden, 2021: Water vapor and lapse rate feedbacks in the climate system. *Rev. Mod. Phys.*, **93**, 045002, <https://doi.org/10.1103/RevModPhys.93.045002>.
- Dahlmann, K., V. Grewe, S. Matthes, and H. Yamashita, 2023: Climate assessment of single flights: Deduction of route specific equivalent CO<sub>2</sub> emissions. *J. Sustainable Transp.*, **17**, 29–40, <https://doi.org/10.1080/15568318.2021.1979136>.
- Dallara, E. S., I. M. Kroo, and I. A. Waitz, 2011: Metric for comparing lifetime average climate impact of aircraft. *AIAA J.*, **49**, 1600–1613, <https://doi.org/10.2514/1.J050763>.
- Deuber, O., M. Sigrun, S. Robert, P. Michael, and L. Ling, 2013: A physical metric-based framework for evaluating the climate trade-off between CO<sub>2</sub> and contrails—The case of lowering aircraft flight trajectories. *Environ. Sci. Policy*, **25**, 176–185, <https://doi.org/10.1016/j.envsci.2012.10.004>.
- Díaz-Francés, E., and F. J. Rubio, 2013: On the existence of a normal approximation to the distribution of the ratio of two independent normal random variables. *Stat. Pap.*, **54**, 309–323, <https://doi.org/10.1007/s00362-012-0429-2>.
- Dietmüller, S., and Coauthors, 2016: A new radiation infrastructure for the Modular Earth Submodel System (MESSy, based on version 2.51). *Geosci. Model Dev.*, **9**, 2209–2222, <https://doi.org/10.5194/gmd-9-2209-2016>.
- Duda, D. P., W. L. Smith Jr., S. Bedka, D. Spangenberg, T. Chee, and P. Minnis, 2023: Impact of COVID-19-related air traffic reductions on the coverage and radiative effects of linear persistent contrails over conterminous United States and surrounding oceanic routes. *J. Geophys. Res. Atmos.*, **128**, e2022JD037554, <https://doi.org/10.1029/2022JD037554>.
- Forster, P., R. S. Freckleton, and K. P. Shine, 1997: On aspects of the concept of radiative forcing. *Climate Dyn.*, **13**, 547–560, <https://doi.org/10.1007/s003820050182>.
- , and Coauthors, 2016: Recommendations for diagnosing effective radiative forcing from climate models for CMIP6. *J. Geophys. Res. Atmos.*, **121**, 12 460–12 475, <https://doi.org/10.1002/2016JD025320>.

- , and Coauthors, 2021: The Earth's energy budget, climate feedbacks and climate sensitivity. *Climate Change 2021: The Physical Science Basis*, V. Masson-Delmotte et al., Eds., Cambridge University Press, 923–1054, <https://doi.org/10.1017/9781009157896.009>.
- Fuglestedt, J., T. K. Berntsen, O. Godal, R. Sausen, K. P. Shine, and T. Skodvin, 2003: Metrics of climate change: Assessing radiative forcing and emission indices. *Climatic Change*, **58**, 267–331, <https://doi.org/10.1023/A:1023905326842>.
- , T. Berntsen, G. Myhre, K. Rypdal, and R. B. Skeie, 2008: Climate forcing from the transport sectors. *Proc. Natl. Acad. Sci. USA*, **105**, 454–458, <https://doi.org/10.1073/pnas.0702958104>.
- , M. T. Lund, S. Kallbekken, B. H. Samset, and D. S. Lee, 2023: A “greenhouse gas balance” for aviation in line with the Paris Agreement. *Wiley Interdiscip. Rev.: Climate Change*, **14**, e839, <https://doi.org/10.1002/wcc.839>.
- , and Coauthors, 2010: Transport impacts on atmosphere and climate: Metrics. *Atmos. Environ.*, **44**, 4648–4677, <https://doi.org/10.1016/j.atmosenv.2009.04.044>.
- Gottelman, A., C.-C. Chen, and C. G. Bardeen, 2021: The climate impact of COVID-19-induced contrail changes. *Atmos. Chem. Phys.*, **21**, 9405–9416, <https://doi.org/10.5194/acp-21-9405-2021>.
- Gregory, J. M., and Coauthors, 2004: A new method for diagnosing radiative forcing and climate sensitivity. *Geophys. Res. Lett.*, **31**, L03205, <https://doi.org/10.1029/2003GL018747>.
- Grewe, V., and Coauthors, 2021: Evaluating the climate impact of aviation emission scenarios towards the Paris agreement including COVID-19 effects. *Nat. Commun.*, **12**, 3841, <https://doi.org/10.1038/s41467-021-24091-y>.
- Hansen, J., and Coauthors, 2005: Efficacy of climate forcings. *J. Geophys. Res.*, **110**, D18104, <https://doi.org/10.1029/2005JD005776>.
- Heymansfield, A. J., D. Baumgardner, P. DeMott, P. Forster, K. Gierens, and B. Kärcher, 2010: Contrail microphysics. *Bull. Amer. Meteor. Soc.*, **91**, 465–472, <https://doi.org/10.1175/2009BAMS2839.1>.
- Hodnebrog, Ø., and Coauthors, 2020: The effect of rapid adjustments to halocarbons and N<sub>2</sub>O on radiative forcing. *npj Climate Atmos. Sci.*, **3**, 43, <https://doi.org/10.1038/s41612-020-00150-x>.
- Huszar, P., and Coauthors, 2013: Modeling the present and future impact of aviation on climate: An AOGCM approach with online coupled chemistry. *Atmos. Chem. Phys.*, **13**, 10 027–10 048, <https://doi.org/10.5194/acp-13-10027-2013>.
- Irvine, E. A., B. J. Hoskins, and K. P. Shine, 2014: A simple framework for assessing the trade-off between the climate impact of aviation carbon dioxide emissions and contrails for a single flight. *Environ. Res. Lett.*, **9**, 064021, <https://doi.org/10.1088/1748-9326/9/6/064021>.
- Jöckel, P., and Coauthors, 2006: The atmospheric chemistry general circulation model ECHAM5/MESSy1: Consistent simulation of ozone from the surface to the mesosphere. *Atmos. Chem. Phys.*, **6**, 5067–5104, <https://doi.org/10.5194/acp-6-5067-2006>.
- , and Coauthors, 2010: Development cycle 2 of the Modular Earth Submodel System (MESSy2). *Geosci. Model Dev.*, **3**, 717–752, <https://doi.org/10.5194/gmd-3-717-2010>.
- , and Coauthors, 2016: Earth System Chemistry integrated Modelling (ESCiMo) with the Modular Earth Submodel System (MESSy) version 2.51. *Geosci. Model Dev.*, **9**, 1153–1200, <https://doi.org/10.5194/gmd-9-1153-2016>.
- Kaiser, J. C., and Coauthors, 2019: Global aerosol modeling with MADE3 (v3.0) in EMAC (based on v2.53): Model description and evaluation. *Geosci. Model Dev.*, **12**, 541–579, <https://doi.org/10.5194/gmd-12-541-2019>.
- Kärcher, B., 2018: Formation and radiative forcing of contrail cirrus. *Nat. Commun.*, **9**, 1824, <https://doi.org/10.1038/s41467-018-04068-0>.
- , J. Hendricks, and U. Lohmann, 2006: Physically based parameterization of cirrus cloud formation for use in global atmospheric models. *J. Geophys. Res.*, **111**, D01205, <https://doi.org/10.1029/2005JD006219>.
- Kästner, M., R. Meyer, and P. Wendling, 1999: Influence of weather conditions on the distribution of persistent contrails. *Meteor. Appl.*, **6**, 261–271, <https://doi.org/10.1017/S1350482799001231>.
- Kaur, H., G. Bala, and A. K. Seshadri, 2023: Why is climate sensitivity for solar forcing smaller than for an equivalent CO<sub>2</sub> forcing? *J. Climate*, **36**, 775–789, <https://doi.org/10.1175/JCLI-D-21-0980.1>.
- Klocke, D., J. Quaas, and B. Stevens, 2013: Assessment of different metrics for physical climate feedbacks. *Climate Dyn.*, **41**, 1173–1185, <https://doi.org/10.1007/s00382-013-1757-1>.
- Klöwer, M., M. R. Allen, D. S. Lee, S. R. Proud, L. Gallagher, and A. Skowron, 2021: Quantifying aviation's contribution to global warming. *Environ. Res. Lett.*, **16**, 104027, <https://doi.org/10.1088/1748-9326/ac286e>.
- Kuebbeler, M., U. Lohmann, J. Hendricks, and B. Kärcher, 2014: Dust ice nuclei effects on cirrus clouds. *Atmos. Chem. Phys.*, **14**, 3027–3046, <https://doi.org/10.5194/acp-14-3027-2014>.
- Kunze, M., M. Godolt, U. Langematz, J. L. Grenfell, A. Hamann-Reinus, and H. Rauer, 2014: Investigating the early Earth faint young Sun problem with a general circulation model. *Planet. Space Sci.*, **98**, 77–92, <https://doi.org/10.1016/j.pss.2013.09.011>.
- Lee, D. S., D. W. Fahey, P. M. Forster, P. J. Newton, R. C. N. Wit, L. L. Lim, B. Owen, and R. Sausen, 2009: Aviation and global climate change in the 21st century. *Atmos. Environ.*, **43**, 3520–3537, <https://doi.org/10.1016/j.atmosenv.2009.04.024>.
- , and Coauthors, 2010: Transport impacts on atmosphere and climate: Aviation. *Atmos. Environ.*, **44**, 4678–4734, <https://doi.org/10.1016/j.atmosenv.2009.06.005>.
- , and Coauthors, 2021: The contribution of global aviation to anthropogenic climate forcing for 2000 to 2018. *Atmos. Environ.*, **244**, 117834, <https://doi.org/10.1016/j.atmosenv.2020.117834>.
- , M. R. Allen, N. Cumpsty, B. Owen, K. P. Shine, and A. Skowron, 2023: Uncertainties in mitigating aviation non-CO<sub>2</sub> emissions for climate and air quality using hydrocarbon fuels. *Environ. Sci. Atmos.*, **3**, 1693–1740, <https://doi.org/10.1039/D3EA00091E>.
- Lelieveld, J., and Coauthors, 2007: Stratospheric dryness: Model simulations and satellite observations. *Atmos. Chem. Phys.*, **7**, 1313–1332, <https://doi.org/10.5194/acp-7-1313-2007>.
- Lewellen, D. C., O. Meza, and W. W. Huebsch, 2014: Persistent contrails and contrail cirrus. Part I: Large-eddy simulations from inception to demise. *J. Atmos. Sci.*, **71**, 4399–4419, <https://doi.org/10.1175/JAS-D-13-0316.1>.
- Li, C., J.-S. von Storch, and J. Marotzke, 2012: Deep-ocean heat uptake and equilibrium climate response. *Climate Dyn.*, **40**, 1071–1086, <https://doi.org/10.1007/s00382-012-1350-z>.
- Lin, G., H. Wan, K. Zhang, Y. Qian, and S. J. Ghan, 2016: Can nudging be used to quantify model sensitivities in precipitation and cloud forcing? *J. Adv. Model. Earth Syst.*, **8**, 1073–1091, <https://doi.org/10.1002/2016MS000659>.

- Lohmann, U., and S. Ferrachat, 2010: Impact of parametric uncertainties on the present-day climate and on the anthropogenic aerosol effect. *Atmos. Chem. Phys.*, **10**, 11 373–11 383, <https://doi.org/10.5194/acp-10-11373-2010>.
- Lund, M. T., B. Aamaas, T. Berntsen, L. Bock, U. Burkhardt, J. S. Fuglestedt, and K. P. Shine, 2017: Emission metrics for quantifying regional climate impacts of aviation. *Earth Syst. Dyn.*, **8**, 547–563, <https://doi.org/10.5194/esd-8-547-2017>.
- Marais, K., S. P. Lukachko, M. Jung, A. Mahashabde, and I. A. Waitz, 2008: Assessing the impact of aviation on climate. *Meteor. Z.*, **17**, 157–172, <https://doi.org/10.1127/0941-2948/2008/0274>.
- Marquart, S., M. Ponater, F. Mager, and R. Sausen, 2003: Future development of contrail cover, optical depth, and radiative forcing: Impacts of increasing air traffic and climate change. *J. Climate*, **16**, 2890–2904, [https://doi.org/10.1175/1520-0442\(2003\)016<2890:FDOCCO>2.0.CO;2](https://doi.org/10.1175/1520-0442(2003)016<2890:FDOCCO>2.0.CO;2).
- Mauritsen, T., and Coauthors, 2012: Tuning the climate of a global model. *J. Adv. Model. Earth Syst.*, **4**, M00A01, <https://doi.org/10.1029/2012MS000154>.
- McCoy, D. T., and Coauthors, 2022: Extratropical shortwave cloud feedbacks in the context of the global circulation and hydrological cycle. *Geophys. Res. Lett.*, **49**, e2021GL097154, <https://doi.org/10.1029/2021GL097154>.
- Megill, L., K. Deck, and V. Grewe, 2024: Alternative climate metrics to the Global Warming Potential are more suitable for assessing aviation non-CO<sub>2</sub> effects. *Commun. Earth Environ.*, **5**, 249, <https://doi.org/10.1038/s43247-024-01423-6>.
- Meraner, K., T. Mauritsen, and A. Voigt, 2013: Robust increase in equilibrium climate sensitivity under global warming. *Geophys. Res. Lett.*, **40**, 5944–5948, <https://doi.org/10.1002/2013GL058118>.
- Minnis, P., D. F. Young, D. P. Garber, L. Nguyen, W. L. Smith Jr., and R. Palikonda, 1998: Transformation of contrails into cirrus during SUCCESS. *Geophys. Res. Lett.*, **25**, 1157–1160, <https://doi.org/10.1029/97GL03314>.
- , U. Schumann, D. R. Doelling, K. M. Gierens, and D. W. Fahey, 1999: Global distribution of contrail radiative forcing. *Geophys. Res. Lett.*, **26**, 1853–1856, <https://doi.org/10.1029/1999GL900358>.
- Myhre, G., and Coauthors, 2013: Anthropogenic and natural radiative forcing. *Climate Change 2013: The Physical Science Basis*, T. F. Stocker et al., Eds., Cambridge University Press, 659–740, <https://doi.org/10.1017/CBO9781107415324.018>.
- Newinger, C., and U. Burkhardt, 2012: Sensitivity of contrail cirrus radiative forcing to air traffic scheduling. *J. Geophys. Res.*, **117**, D10205, <https://doi.org/10.1029/2011JD016736>.
- O'Connor, F. M., B. T. Johnson, O. Jamil, T. Andrews, J. P. Mulcahy, and J. Manners, 2022: Apportionment of the pre-industrial to present-day climate forcing by methane using UKESM1: The role of the cloud radiative effect. *J. Adv. Model. Earth Syst.*, **14**, e2022MS002991, <https://doi.org/10.1029/2022MS002991>.
- Penner, J., D. H. Lister, D. J. Griggs, D. J. Dokken, and M. McFarland, Eds., 1999: *Aviation and the Global Atmosphere*. Cambridge University Press, 373 pp.
- Ponater, M., 2010: Distinctive efficacies of the components contributing to total aviation climate impact. *Proc. Second Int. Conf. on Transport, Atmosphere and Climate (TAC-2)*, Aachen, Germany and Maastricht, Netherlands, Deutsches Zentrum für Luft- und Raumfahrt, 227–232, <https://elib.dlr.de/65284/>.
- , S. Marquart, R. Sausen, and U. Schumann, 2005: On contrail climate sensitivity. *Geophys. Res. Lett.*, **32**, L10706, <https://doi.org/10.1029/2005GL022580>.
- , S. Pechtl, R. Sausen, U. Schumann, and G. Hüttig, 2006: Potential of the cryoplane technology to reduce aircraft climate impact: A state-of-the-art assessment. *Atmos. Environ.*, **40**, 6928–6944, <https://doi.org/10.1016/j.atmosenv.2006.06.036>.
- , M. Bickel, L. Bock, and U. Burkhardt, 2021: Towards determining the contrail cirrus efficacy. *Aerospace*, **8**, 42, <https://doi.org/10.3390/aerospace8020042>.
- Quaas, J., E. Gryspeerdt, R. Vautard, and O. Boucher, 2021: Climate impact of aircraft-induced cirrus assessed from satellite observations before and during COVID–19. *Environ. Res. Lett.*, **16**, 064051, <https://doi.org/10.1088/1748-9326/abf686>.
- Rädel, G., and K. P. Shine, 2008: Radiative forcing by persistent contrails and its dependence on cruise altitudes. *J. Geophys. Res.*, **113**, D07105, <https://doi.org/10.1029/2007JD009117>.
- Ramaswamy, V., and Coauthors, 2018: Radiative forcing of climate: The historical evolution of the radiative forcing concept, the forcing agents and their quantification, and applications. *A Century of Progress in Atmospheric and Related Sciences: Celebrating the American Meteorological Society Centennial, Meteor. Monogr.*, No. 59, Amer. Meteor. Soc., <https://doi.org/10.1175/AMSMONOGRAPHIS-D-19-0001.1>.
- Rap, A., P. M. Forster, J. M. Haywood, A. Jones, and O. Boucher, 2010: Estimating the climate impact of linear contrails using the UK Met Office climate model. *Geophys. Res. Lett.*, **37**, L20703, <https://doi.org/10.1029/2010GL045161>.
- Rayner, N. A., D. E. Parker, E. B. Horton, C. K. Folland, L. V. Alexander, D. P. Rowell, E. C. Kent, and A. Kaplan, 2003: Global analyses of sea surface temperature, sea ice, and night marine air temperature since the late nineteenth century. *J. Geophys. Res.*, **108**, 4407, <https://doi.org/10.1029/2002JD002670>.
- Richardson, T. B., and Coauthors, 2019: Efficacy of climate forcings in PDRMIP models. *J. Geophys. Res. Atmos.*, **124**, 12 824–12 844, <https://doi.org/10.1029/2019JD030581>.
- Rieger, V. S., S. Dietmüller, and M. Ponater, 2017: Can feedback analysis be used to uncover the physical origin of climate sensitivity and efficacy differences? *Climate Dyn.*, **49**, 2831–2844, <https://doi.org/10.1007/s00382-016-3476-x>.
- Righi, M., and Coauthors, 2020: Coupling aerosols to (cirrus) clouds in the global EMAC-MADE3 aerosol-climate model. *Geosci. Model Dev.*, **13**, 1635–1661, <https://doi.org/10.5194/gmd-13-1635-2020>.
- , J. Hendricks, and C. G. Beer, 2021: Exploring the uncertainties in the aviation soot–cirrus effect. *Atmos. Chem. Phys.*, **21**, 17 267–17 289, <https://doi.org/10.5194/acp-21-17267-2021>.
- , —, and S. Brinkop, 2023: The global impact of the transport sectors on the atmospheric aerosol and the resulting climate effects under the Shared Socioeconomic Pathways (SSPs). *Earth Syst. Dyn.*, **14**, 835–859, <https://doi.org/10.5194/esd-14-835-2023>.
- Roeckner, E., and Coauthors, 2006: Sensitivity of simulated climate to horizontal and vertical resolution in the ECHAM5 atmosphere model. *J. Climate*, **19**, 3771–3791, <https://doi.org/10.1175/JCLI3824.1>.
- Sausen, R., and Coauthors, 2005: Aviation radiative forcing in 2000: An update on IPCC (1999). *Meteor. Z.*, **14**, 555–561, <https://doi.org/10.1127/0941-2948/2005/0049>.
- Schneider, T., C. M. Kaul, and K. G. Pressel, 2019: Possible climate transitions from breakup of stratocumulus decks under greenhouse warming. *Nat. Geosci.*, **12**, 163–167, <https://doi.org/10.1038/s41561-019-0310-1>.

- Schumann, U., 2012: A contrail cirrus prediction model. *Geosci. Model Dev.*, **5**, 543–580, <https://doi.org/10.5194/gmd-5-543-2012>.
- , and K. Graf, 2013: Aviation-induced cirrus and radiation changes at diurnal timescales. *J. Geophys. Res. Atmos.*, **118**, 2404–2421, <https://doi.org/10.1002/jgrd.50184>.
- , and B. Mayer, 2017: Sensitivity of surface temperature to radiative forcing by contrail cirrus in a radiative-mixing model. *Atmos. Chem. Phys.*, **17**, 13833–13848, <https://doi.org/10.5194/acp-17-13833-2017>.
- , —, K. Graf, and H. Mannstein, 2012: A parametric radiative forcing model for contrail cirrus. *J. Appl. Meteor. Climatol.*, **51**, 1391–1406, <https://doi.org/10.1175/JAMC-D-11-0242.1>.
- , J. E. Penner, Y. Chen, C. Zhou, and K. Graf, 2015: Dehydration effects from contrails in a coupled contrail–climate model. *Atmos. Chem. Phys.*, **15**, 11179–11199, <https://doi.org/10.5194/acp-15-11179-2015>.
- , L. Bugliaro, A. Dörnbrack, R. Baumann, and C. Voigt, 2021: Aviation contrail cirrus and radiative forcing over Europe during 6 months of COVID–19. *Geophys. Res. Lett.*, **48**, e2021GL092771, <https://doi.org/10.1029/2021GL092771>.
- Sherwood, S. C., and Coauthors, 2020: An assessment of Earth’s climate sensitivity using multiple lines of evidence. *Rev. Geophys.*, **58**, e2019RG000678, <https://doi.org/10.1029/2019RG000678>.
- Shindell, D. T., 2014: Inhomogeneous forcing and transient climate sensitivity. *Nat. Climate Change*, **4**, 274–277, <https://doi.org/10.1038/nclimate2136>.
- , G. Faluvegi, L. Rotsteyn, and G. Milly, 2015: Spatial patterns of radiative forcing and surface temperature response. *J. Geophys. Res. Atmos.*, **120**, 5385–5403, <https://doi.org/10.1002/2014JD022752>.
- Shine, K. P., 2015: Radiative forcing and climate change. *Encyclopedia of Aerospace Engineering*, R. Blockley and W. Shyy, Eds., Wiley, 1–11, <https://doi.org/10.1002/9780470686652.eae526.pub2>.
- , J. Cook, E. J. Highwood, and M. M. Joshi, 2003: An alternative to radiative forcing for estimating the relative importance of climate change mechanisms. *Geophys. Res. Lett.*, **30**, 2047, <https://doi.org/10.1029/2003GL018141>.
- Smith, C. J., and Coauthors, 2018: Understanding rapid adjustments to diverse forcing agents. *Geophys. Res. Lett.*, **45**, 12 023–12 031, <https://doi.org/10.1029/2018GL079826>.
- , and Coauthors, 2020: Effective radiative forcing and adjustments in CMIP6 models. *Atmos. Chem. Phys.*, **20**, 9591–9618, <https://doi.org/10.5194/acp-20-9591-2020>.
- Soden, B. J., I. M. Held, R. Colman, K. M. Shell, J. T. Kiehl, and C. A. Shields, 2008: Quantifying climate feedbacks using radiative kernels. *J. Climate*, **21**, 3504–3520, <https://doi.org/10.1175/2007JCLI2110.1>.
- Stecher, L., F. Winterstein, M. Dameris, P. Jöckel, M. Ponater, and M. Kunze, 2021: Slow feedbacks resulting from strongly enhanced atmospheric methane mixing ratios in a chemistry–climate model with mixed-layer ocean. *Atmos. Chem. Phys.*, **21**, 731–754, <https://doi.org/10.5194/acp-21-731-2021>.
- Stevens, B., and Coauthors, 2019: DYAMOND: The DYNAMics of the Atmospheric general circulation Modeled On Non-hydrostatic Domains. *Prog. Earth Planet. Sci.*, **6**, 61, <https://doi.org/10.1186/s40645-019-0304-z>.
- , and Coauthors, 2020: The added value of large-eddy and storm-resolving models for simulating clouds and precipitation. *J. Meteor. Soc. Japan*, **98**, 395–435, <https://doi.org/10.2151/jmsj.2020-021>.
- Stier, P., and Coauthors, 2005: The aerosol-climate model ECHAM5-HAM. *Atmos. Chem. Phys.*, **5**, 1125–1156, <https://doi.org/10.5194/acp-5-1125-2005>.
- Stuber, N., R. Sausen, and M. Ponater, 2001: Stratosphere adjusted radiative forcing calculations in a comprehensive climate model. *Theor. Appl. Climatol.*, **68**, 125–135, <https://doi.org/10.1007/s007040170041>.
- , M. Ponater, and R. Sausen, 2005: Why radiative forcing might fail as a predictor of climate change. *Climate Dyn.*, **24**, 497–510, <https://doi.org/10.1007/s00382-004-0497-7>.
- , P. Forster, G. Rädcl, and K. Shine, 2006: The importance of the diurnal and annual cycle of air traffic for contrail radiative forcing. *Nature*, **441**, 864–867, <https://doi.org/10.1038/nature04877>.
- Sun, J., K. Zhang, H. Wan, P.-L. Ma, Q. Tan, and S. Zhang, 2019: Impact of nudging strategy on the climate representativeness and hindcast skill of constrained EAMv1 simulations. *J. Adv. Model. Earth Syst.*, **11**, 3911–3933, <https://doi.org/10.1029/2019MS001831>.
- Sundqvist, H., 1978: A parameterization scheme for non-convective condensation including prediction of cloud water content. *Quart. J. Roy. Meteor. Soc.*, **104**, 677–690, <https://doi.org/10.1002/qj.49710444110>.
- Teoh, R., U. Schumann, A. Majumdar, and M. E. J. Stettler, 2020a: Mitigating the climate forcing of aircraft contrails by small-scale diversions and technology adoption. *Environ. Sci. Technol.*, **54**, 2941–2950, <https://doi.org/10.1021/acs.est.9b05608>.
- , —, and M. E. J. Stettler, 2020b: Beyond contrail avoidance: Efficacy of flight altitude changes to minimise contrail climate forcing. *Aerospace*, **7**, 121, <https://doi.org/10.3390/aerospace7090121>.
- Unterstrasser, S., and I. Sölch, 2013: Numerical modeling of contrail cluster formation. *Third Int. Conf. on Transport, Atmosphere and Climate*, Prien am Chiemsee, Germany, 114–119, <https://elib.dlr.de/87363/>.
- , K. Gierens, I. Sölch, and M. Lainer, 2017: Numerical simulations of homogeneously nucleated natural cirrus and contrail-cirrus. Part 2: Interaction on local scale. *Meteor. Z.*, **26**, 643–661, <https://doi.org/10.1127/metz/2016/0780>.
- Verma, P., and U. Burkhardt, 2022: Contrail formation within cirrus: ICON-LEM simulations of the impact of cirrus cloud properties on contrail formation. *Atmos. Chem. Phys.*, **22**, 8819–8842, <https://doi.org/10.5194/acp-22-8819-2022>.
- Vial, J., J.-L. Dufresne, and S. Bony, 2013: On the interpretation of inter-model spread in CMIP5 climate sensitivity estimates. *Climate Dyn.*, **41**, 3339–3362, <https://doi.org/10.1007/s00382-013-1725-9>.
- Vogel, R., A. L. Albright, J. Vial, G. George, B. Stevens, and S. Bony, 2022: Strong cloud–circulation coupling explains weak trade cumulus feedback. *Nature*, **612**, 696–700, <https://doi.org/10.1038/s41586-022-05364-y>.
- Wilkerson, J. T., M. Z. Jacobson, A. Malwitz, S. Balasubramanian, R. Wayson, G. Fleming, A. D. Naiman, and S. K. Lele, 2010: Analysis of emission data from global commercial aviation: 2004 and 2006. *Atmos. Chem. Phys.*, **10**, 6391–6408, <https://doi.org/10.5194/acp-10-6391-2010>.
- Yamashita, H., F. Yin, V. Grewe, P. Jöckel, S. Matthes, B. Kern, K. Dahlmann, and C. Frömming, 2020: Newly developed aircraft routing options for air traffic simulation in the chemistry–climate model EMAC 2.53: AirTraf 2.0. *Geosci. Model Dev.*, **13**, 4869–4890, <https://doi.org/10.5194/gmd-13-4869-2020>.

- Yoshimori, M., and A. J. Broccoli, 2008: Equilibrium response of an atmosphere–mixed layer ocean model to different radiative forcing agents: Global and zonal mean response. *J. Climate*, **21**, 4399–4423, <https://doi.org/10.1175/2008JCLI2172.1>.
- Zelinka, M. D., S. A. Klein, and D. L. Hartmann, 2012: Computing and partitioning cloud feedbacks using cloud property histograms. Part I: Cloud radiative kernels. *J. Climate*, **25**, 3715–3735, <https://doi.org/10.1175/JCLI-D-11-00248.1>.
- , T. A. Myers, D. T. McCoy, S. Po-Chedley, P. M. Caldwell, P. Ceppi, S. A. Klein, and K. E. Taylor, 2020: Causes of higher climate sensitivity in CMIP6 models. *Geophys. Res. Lett.*, **47**, e2019GL085782, <https://doi.org/10.1029/2019GL085782>.
- Zhou, C., M. Wang, M. D. Zelinka, Y. Liu, Y. Dong, and K. C. Armour, 2023: Explaining forcing efficacy with pattern effect and state dependence. *Geophys. Res. Lett.*, **50**, e2022GL101700, <https://doi.org/10.1029/2022GL101700>.